Czech Technical University

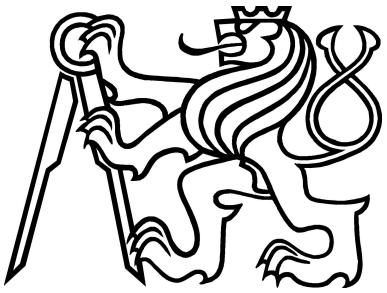

Master Thesis

Gust Load Alleviation System for BWB (Blended Wing Body) Flexible Aircraft

Author:

Mushfiqul Alam

Supervisor:

Dr. Martin Hromcik

A thesis submitted in fulfilment of the requirements for the Master Degree

in the

Faculty of Electrical Engineering

Department of Control Engineering

May 2013

Czech Technical University in Prague
Faculty of Electrical Engineering

Department of Control Engineering

DIPLOMA THESIS ASSIGNMENT

Student: **Mushfiqul Mohammad Alam**

Study programme: Cybernetics and Robotics
Specialisation: Systems and Control

Title of Diploma Thesis: **Gust load alleviation system for BWB flxible aircraft.**

Guidelines:

The goal is to develop a combined feedforward / feedback control law to reduce the loads in the wingroot excited by gust. While the feedforward action is used for increased performance compared to purely feedback controls, the feedback part is implemented with emphasis on increased robustness of the overal solution w.r.t. aircraft and/or gust parameters uncertainties.

1. Get familiar with the simulation model of a flexible high capacity BWB airliner.
2. Develop simple feedback controllers for gust load alleviation.
3. Assess their performance in combination with an existing feedforward control.
4. Tune / redesign the feedback part to meet the expected improvements over the feedforward part, namely the enhanced robustness of the solution.

Bibliography/Sources:

Literature: S. Skogestad, Multivariable feedback control, MsGraw Hill, NY, 2001

Diploma Thesis Supervisor: Ing. Martin Hromčík, Ph.D.

Valid until the summer semester 2013/2014

prof. Ing. Michael Šebek, DrSc.
Head of Department

L.S.

prof. Ing. Pavel Ripka, CSc.
Dean

Prague, January 15, 2013

Declaration of Authorship

I, Mushfiqul Alam, declare that this thesis titled, 'Gust Load Alleviation System for BWB (Blended Wing Body) Flexible Aircraft' and the work presented in it are my own. I confirm that:

- This work was done wholly or mainly while in candidature for a research degree at this University.
- Where any part of this thesis has previously been submitted for a degree or any other qualification at this University or any other institution, this has been clearly stated.
- Where I have consulted the published work of others, this is always clearly attributed.
- Where I have quoted from the work of others, the source is always given. With the exception of such quotations, this thesis is entirely my own work.
- I have acknowledged all main sources of help.
- Where the thesis is based on work done by myself jointly with others, I have made clear exactly what was done by others and what I have contributed myself.

Signed: _____

Place and Date: _____

"In the Name of Allah, The Most Merciful, The Most Kind."

CZECH TECHNICAL UNIVERSITY

Abstract

Faculty of Electrical Engineering
Department of Control Engineering

Master Degree

Gust Load Alleviation System for BWB Flexible Aircraft

by Mushfiqul Alam

A new BWB concept aircraft was developed to meet the ACARE 2020 vision. A patented feedforward controller was designed earlier at EADS Innovation Works to alleviate the gust loading, but it was not robust over shorter gust lengths and mass cases. This thesis focused on the controller design for Gust Load Alleviation System (GLAS)for BWB Flexible Aircraft which worked together with feedforward controller.

The thesis aimed towards improving the performance of the feedforward controller making it robust over shorther gust lengths. Emphasis was given on the reduction of wing root moments keeping the overall stability of the aircraft to an acceptable level. For the control design, the non linear actuators model of the BWB aircraft was linearised with $2nd$ order approximation. New GLAS controller was designed to work together with feedforward controller using different design techniques namely, nominal SISO and modern Linear Quadratic Regulator and $\mathcal{H}_\infty$ controller.

The result shows that the nominal SISO controller gives the best performance compared to LQ and $\mathcal{H}_\infty$ controller in terms of reduction of wing root moments, which provides structural benefits.

Acknowledgements

First and foremost, I would like to express my gratitude to my supervisor Dr. Martin Hromcik for giving me the opportunity to work on this interesting topic and for his interminable support and guidance. I would also like to thank him for creating perfect conditions for my research, for encouragement and motivation and for introducing me to the world of research.

I also wish to thank Dr. Tomas Hanis for his remote advising on the NACRE model. In the Department of Control Engineering, I am specially grateful to Prof. Jan Stecha, Dr. Zdenek Hurak and Dr. Jan Rohac for their teaching efforts and the technical discussions we had throughout my stay in the department.

My thanks also go to everyone who is involved in the SpaceMaster program at Lulea University of Technology in Sweden, and Julius-Maximilian's University of Wuerzburg in Germany. Thanks goes to European Commission for making my study possible through the Erasmus Mundus Scholarship and supporting the SpaceMaster programme. I also thank EADS Innovation Works for agreeing to provide me with the NACRE aircraft model.

Probably I have forgotten to mention a lot of individual, but you are always in my thoughts. Finally I would like to thank all of my friends from SpaceMaster Round 7 for gifting me with a wonderful time.

Thank you all,

Mushfiqul Alam

Dedicated to Ammu (mother), Momarrema Alam, Abbu (father), Mostafizul Alam and to all my family members.

Contents

List of Figures

List of Tables

Abbreviations

ACFA	Active Control For Flexible Aircraft
ACARE	Advisory Council for Aeronautics Research in Europe
EADS	The European Aeronautic Defence and Space Company
NACRE	New Aircraft Concept Research
MIMO	Multiple Input Multiple Output
SISO	Single Input Single Output
TUV	Technical University of Vienna
VELA	Very Efficient Large Aircraft

Symbols

α	Angle of Attack	$\circ$ or rad
θ	Pitch Angle	$\circ$ or rad
q	Pith Rate	rad/s
η_z	Wing tip Acceleration	g (ms^{-2})
M_x	Wing Root Bending Moment	Nm
M_y	Wing Root Torsional Moment	Nm
F_z	Wing Root Cut Force	N

Chapter 1

Introduction

The current design and mission requirements for military and commercial transport aircrafts are such that the resulting configurations of such vehicles requires the use of thin lifting surfaces, long and slender fuselages, low mass fraction structures, high stress design levels, and low dynamic load factors. In turn, those features have resulted in aircraft which are structurally light and flexible.

Such aircraft can develop large values of displacement and acceleration as a result of structural deflection, in addition to those components of displacement and acceleration which arise owing to the rigid body motion of the aircraft. Such structural deflections may occur as a result of aircraft's passage through turbulent air.

Aircraft motion of this kind can result in a reduction of the structural life of the airframe because of the large dynamic loads and the consequent high levels of stress. The amplitude of the aircraft's response, caused by gust-induced structural flexibility, depends upon either the amount of energy transferred from the gust disturbance to the structural bending modes or, if any energy is absorbed from the gust, the dissipation of that energy by some form of damping. When the amplitude of the response of the elastic motion is such that it compares with that of the rigid body motion, there can be an interchange between the rigid body energy and the elastic energy to the detriment of the flying qualities of the aircraft.

1.1 Motivations

ACFA 2020 was a collaborative research project funded by the European Commission under the seventh research framework programme (FP7). The project dealt with innovative active control concepts for ultra efficient 2020 aircraft configurations like the blended wing body (BWB) aircraft. The Advisory Council for Aeronautics Research in Europe (ACARE) formulated the "ACARE vision 2020", which aims for:

- 50 % reduced fuel consumption and related CO2 emissions per passenger-kilometre.
- Reduction of external noise by 4-5 dB and by 10 dB per operation in the short and long terms, respectively. To meet these goals is very important to minimise the environmental impact of air traffic but also of vital interest for the aircraft industry to enable future growth.

Blended Wing Body type aircraft configurations are seen as the most promising future concept to fulfil the ACARE vision 2020 goals because aircraft's efficiency can be dramatically increased through minimisation of the wetted area and by reduced structural weight. With development of light weight flexible aircraft structure the active control issues became significantly important. Minimization of structural deflections due to air turbulence such as gusts is essentially crucial with respect to wing bending and torsional moments.

1.2 Project Goals and Objective

Structural mass saving by active control law is common nowadays, a trend being widely investigated. Main task of this diploma thesis is to design feedback part of gust load alleviation system for Blended Wing Body aircraft (BWB) to make feed forward part more insensitive to variation of gust lengths. Design will be done by classical approaches (root locus, nominal frequency shaping) and later on by

modern techniques (H2 optimization as a LQ, model matching and finally robust loop shaping). Results will be design based on mathematical model of airliner containing flexible modes description and finally validated on high precision model in Matlab Simulink. Master thesis will be done in following points:

- Model acceptance: receiving of models including design, validation and Matlab Simulink models. Installing necessary prerequisites and validation of models.
- Mathematical model analysis: sensitivity analysis, robust analysis. Inputs and outputs selection optimization.
- Nominal control law design: design of nominal SISO control law to full fill extra insensitivity requirements, by using classical approaches (root locus, nominal frequency shaping).
- Validation of nominal control law: based on Matlab Simulink model.
- Design of control law by using modern approaches: $\mathcal{H}_2$ and $\mathcal{H}_\infty$ approaches.
- Validation of designed control law and final assessment.

1.3 Literature Review

The Advisory Council for Aeronautics Research in Europe (ACARE) formulated the "ACARE vision 2020", which aimed for 50% reduced fuel consumption and related CO2 emissions per passenger-kilometre and reduction of external noise by 10dB. To meet the ACARE vision Blended wing body aircraft is the most promising architecture. And therefore ACFA2020 project was undertaken under the 7th European Commission frame work.

BWB type aircrafts are promising for high efficiency due to a smaller wetted area compared to classical tube/wing configuration and also due to a lower structural weight. The BWB configuration also offers a great potential for the minimization

of noise signature through integration of the engine over the rear fuselage or in the airframe and also due to the generally higher wing area/weight ratio, which allows for a simplified high-lift system [10][11][15].

First of all, European research on highly efficient aircraft configurations in the projects VELA and NACRE [6] were concentrated on very large aircrafts for more than 700 passengers but the biggest market share in long haul flights is taken by smaller mid-size. As a result ACFA 2020 deals with the design of an ultra-efficient mid-size aircraft. Hereby, blended wing body configurations (BWB) has been compared to a more conventional aircraft with ultra wide body and carry through wing box (CWB).

Due to the unconventional placement of control surfaces, BWB type aircrafts require new multi-channel design methods and architectures in particular for active loads and vibration control. Moreover new promising active control concepts such as adaptive feed-forward control and neural network control were investigated in ACFA 2020.

The control concepts are applied to two aircraft models. In a first step a large flying wing aircraft for 750 passengers designed in the VELA and NACRE projects [6] were used. For that purpose an aero-elastic model had been generated based on the geometry and structural design as performed in the NACRE project. Main application case was a newly designed ultra-efficient 450 passenger aircraft.

For this 450 passenger aircraft a pre-design for a flying wing and an ultra-wide body fuselage aircraft with carry-through wing box have been performed and both designs have been compared in particular with respect to fuel efficiency. Due to the significant better fuel efficiency the Blended Wing Body design has been retained for the further work in the project. The main objective of the designed control systems was to reduce structural vibrations and unwanted rigid body motions on the one hand, and gust and manoeuvre loads on the other.

1.3.1 Summary of Conceptual Aircraft Design

Conceptual designs for two configurations, a 450 passenger blended wing body (BWB) and an ultra-wide-body aircraft with carry through wingbox (CWB), were performed by Technical University of Munich and AIRBUS [7]. Both aircrafts were designed for the same mission roughly defined by the following parameters:

Long Range Cruise Mach number: 0.85
Maximum range at Max Pax Payload: 7200nm
Approach speed should be $<$ 150kt
Maximum operating Mach number MMO: 0.89
Maximum operating speed VMO: 340kts CAS
Max cruise altitude: 43100ft

The concurrent design was mainly done to compare the BWB configuration to a more conventional design in particular with respect to fuel efficiency. It turned out that the BWB aircraft shows about 13 % better fuel efficiency compared to the CWB aircraft which is mainly due to lower weight of the BWB and better aerodynamic performance. Therefore the BWB configuration was retained for the further work on active control concepts [7].

FIGURE 1.1: ACFA 2020 aircraft configurations BWB (left) and CWB (right)[1].

The final BWB configuration has a very blended shape between the centre body and the outer wing in order to get a smooth load & lift distribution along the blended wing span. A quite high sweep and aft position of the wing is important to make the aircraft stable. The BWB provides a lot of space underneath the

cabin for the centre tank and so it can be efficiently used to trim the aircraft during cruise.

However, this makes the fuel system safety critical because it must be operational to keep the aircraft centre of gravity within an acceptable range. The longitudinal control is done by rear elevons located both on the centre body and on the wing (except aft of the engine pylons). The area dedicated to those movables is rather high in order to provide sufficient control authority. The lateral control is critical on this aircraft, especially in the one engine out case, and is achieved by split ailerons and rather high winglets equipped with a rudder. Details about the fuel management system and design of BWB can be found in the reference [7] and [8].

1.3.2 Sound Level

Two engines are located on the upper side of the centre body so it was expected to provide efficient shielding for the fan noise. However, a small study on interior noise comfort was performed with respect to turbulent boundary layer noise, which is the major noise source in cruise condition. Statistical energy analysis was applied for a portion of the cargo/cabin area, whereby some optimisation of the cabin treatment was performed. Results showed that BWB has significantly lower noise levels than the CWB and both aircrafts are quieter than a generic conventional single aisle aircraft configuration which was used as an additional reference [1]. The mean overall sound pressure level of the BWB is about 3dB below the sound pressure level of the CWB configuration which is quite significant. The main reason behind is the large distance between the cabin and the outer skin which leads to a high transmission loss already at low frequencies. With respect to cabin noise one can conclude that the BWB configuration is quite favourable [1] [6].

1.3.3 Development of BWB concept

Defining the pressurized passenger cabin for a very large airplane offers two challenges. First, the square-cube law shows that the cabin surface area per passenger

available for emergency egress decreases with increasing passenger count. Second, cabin pressure loads are most efficiently taken in hoop tension. Thus, the early study began with an attempt to use circular cylinders for the fuselage pressure vessel, as shown in Figure 1.2, along with the corresponding. First cut at the airplane geometry. The engines are buried in the wing root, and it was intended that passengers could egress from the sides of both the upper and lower levels. Clearly, the concept was headed back to a conventional tube and wing configuration. Therefore, it was decided to abandon the requirement for taking pressure loads in hoop tension and to assume that an alternate efficient structural concept could be developed. Removal of this constraint became pivotal for the development of the BWB [2].

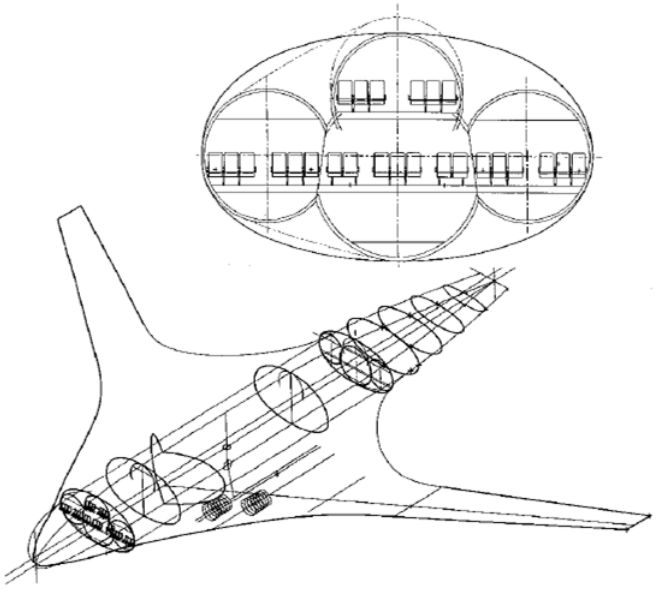

FIGURE 1.2: Early configuration with cylindrical pressure vessel and engines buried in the wing root [2].

Passenger cabin definition became the origin of the design, with the hoop tension structural requirement deleted. Three canonical forms shown in Figure 1.3, each sized to hold 800 passengers, were considered. The sphere has minimum surface area; however, it is not streamlined. Two canonical streamlined options include the conventional cylinder and a disk, both of which have nearly equivalent surface area. Next, each of these fuselages is placed on a wing that has a total surface

area of 15,000 ft^2 . Now the effective masking of the wing by the disk fuselage results in a reduction of total aerodynamic wetted area of 7000 ft^2 compared to the cylindrical fuselage plus wing geometry, as shown in Figure 1.4. Next, adding engines (Figure 1.5) provides a difference in total wetted area of 10,200 ft^2. Weight and balance require that the engines be located aft on the disk configuration. Finally, adding the required control surfaces to each configuration as shown in Figure1.6 results in a total wetted area difference of 14,300 ft^2, or a reduction of 33%. Because the cruise lift to drag ratio is related to the wetted area aspect ratio, $b^2 = S_{wet}$, the BWB configuration implied a substantial improvement in aerodynamic efficiency [2].

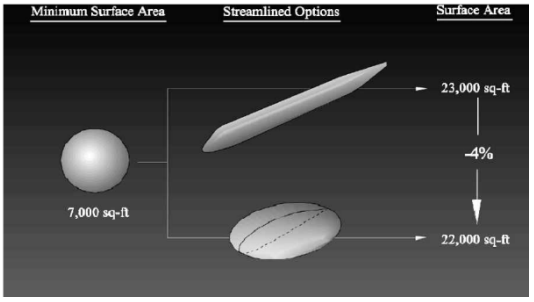

FIGURE 1.3: Effect of body type on surface area [2].

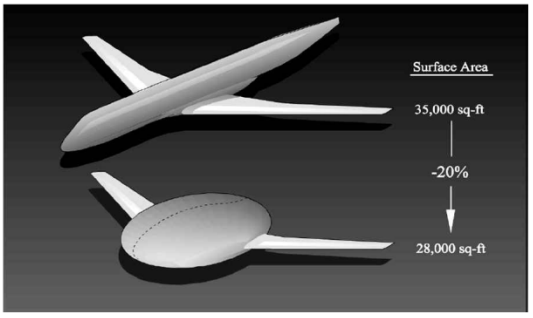

FIGURE 1.4: Effect of wing/body integration on surface area [2].

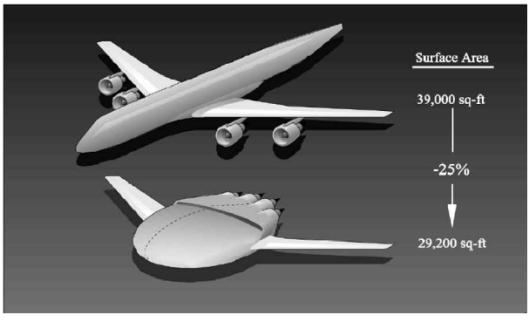

FIGURE 1.5: Effect of engine installation on surface area [2]

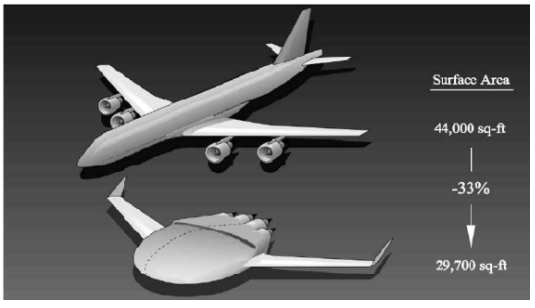

FIGURE 1.6: Effect of controls integration on surface area [2].

The disk fuselage configuration sketched in Figure 1.6 has been used to describe the germination of the BWB concept. The fuselage is also a wing, an inlet for the engines, and a pitch control surface. Verticals provide directional stability, control, and act as winglets to increase the effective aspect ratio. Blending and

smoothing the disk fuselage into the wing achieved transformation of the sketch into a realistic airplane configuration. In addition, a nose bullet was added to offer cockpit visibility. This also provides additional effective wing chord at the centreline to offset compressibility drag due to the unsweeping of the isobars at the plane of symmetry [2].

1.4 Thesis Outline

This thesis is focused mainly on the design of a new controller which will increase the robustness of the feedforward controller for Gust Load Alleviation System (GLAS). Primary computational tool for the design was MATLAB and Simulink. The Model of the aircraft was provided by EADS Innovation Works, Munich. Bases on the controller performance in terms of the reduction of wing root bending the best controller design was justified.

Chapter 2 of the thesis contains discussion on mathematical and theoretical model that has been used to carry out the controller design. The methods of calculating the optimal control solutions are considered in this section.

Chapter 3 of the thesis focuses on the validation of the model provided by the industry, with MATLAB model. It accounts for the assumptions of sensor delays and non-linear actuator model to linear state-space model.

Chapter 4 describes the method of designing different controllers and their results based on different gust lengths and mass cases.

Chapter 5 presents a complete description and comparison of the data. It provides a comaprative analysis of different controllers.

Chapter 6 concludes the final result of the GLAS controller and is presented along with the summarised key findings of the thesis. It also indicated the future works that could be done on the topic.

Chapter 2

Mathematical Theory and Model Generation

2.1 Feedforward Control with Feedback

Feedforward together with feedback control has significantly improved performance when there is a major measurable disturbance to a dynamic system compared to only feedback control. In theory assuming ideal condition feedforward control can completely eliminate the effect of the measured disturbance of the system output [3] [9]. Even when there are modelling errors feedforward control reduces the effect of the disturbance on the system output better than feedback control alone.

Feedforward control is always used along with feedback control because a feedback control system is required to track set point changes and to suppress unmeasured disturbances that are always present in any real process. From Figure 2.1 it can be seen that the feedforward part of the control system does not affect the stability of the feedback system and that each system can be designed independently.

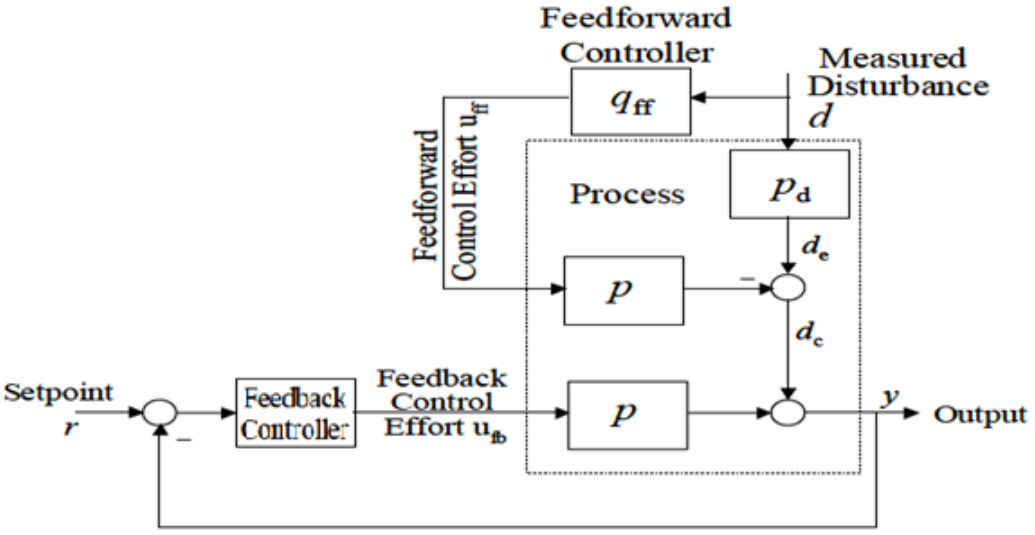

FIGURE 2.1: Feedforward plus feedback control structure [3].

2.1.1 Controller Design with Perfect Compensation

The transfer function between the process put y and the measured disturbance d from Figure 2.1 is

$$y(s) = \frac{d_c}{1 + K * p} = \frac{(p_d - pq_{ff})d}{1 + K * p} \tag{2.1}$$

where K is the feedback controller. To the effect of the measured disturbance, it is needed to choose q_{ff} so that

$$(p_d - pq_{ff})d = 0 \tag{2.2}$$

If the deadtime and relative order of p_d are both greater than those of p, and p has no right half plane zeros, then q_{ff} can be chosen as

$$q_{ff} = \widetilde{p}^{-1}\widetilde{p}_d \tag{2.3}$$

$\sim$ over a process transfer function indicates that it is a model of the process.

Whenever the relative order of $\widetilde{p}_d(s)$ is less than or equal to that of $\widetilde{p}(s)$, then the noise amplification can be reduced by adding a filter, so the equation 2.3 becomes:

$$q_{ff} = \widetilde{p}^{-1}\widetilde{p}_d f; f \equiv \frac{1}{(\epsilon s + 1)^r} \tag{2.4}$$

The order r of the filter f is either the relative order of $\widetilde{p}^{-1}\widetilde{p}_d(s)$ or 0 if the relative order of $\widetilde{p}^{-1}\widetilde{p}_d$ is equal or less than zero. The filter time constant $\epsilon$is chosen to limit noise amplification.

2.2 Optimal Control

Optimal control theory is a mathematical optimization method for deriving control technique. Any dynamical system can be modelled ordinary differential equations and can be (ODE) and takes the form

$$\dot{x}(t) = f(x(t), u(t)); x(0) = x_0; t \in [0, T] \tag{2.5}$$

in which the map $f : R^n \times R^m \to R^n$ is a vector modelling the controlled dynamics. Vector x denotes the dynamical state and is allowed to assume values in a set $X \subseteq R^n$, with time derivative $\dot{x} \in R^n$ governed by f. The independent time variable t is between 0 and terminal time T. Vector u denotes the control and takes its value in a set $U \subseteq R^m$. Both the state and the control are functions of time, namely $x = x(t), u = u(t)$. At the initial time $t = 0$, the state take the initial value x_0 in a set $X_0 \subseteq R^n$. Similarly, at the terminal time, the state takes the terminal value x_T in a set $X^T \subseteq R^n$. To define what is meant by a solution or a response of the control system, lets fix the control to a constant value, $u(t) \equiv a \in U$. A solution $x(t)$ of the control system in equation 2.5, (also called state trajectory) over the interval $[0, T]$ is an absolutely continuous function

of time that is differentiable almost everywhere such that

$$x(t) = x_0 + \int_0^t f(x(s), a)ds \tag{2.6}$$

It is clear that the state trajectory can be "controlled" by changing the constant value a through time by some function $u(t)$, called control trajectory. The existence and uniqueness of such solutions can be guaranteed under some regularity assumptions imposed on both the vector field and the control function. In cases where the vector field is time independent, assuming that the map $f : R^n \times R^m \to R^n$ is Lipschitz is sufficient. We assume that $f(x(s), a)$ is a measurable function of s. The state trajectory $x(t)$ is then absolutely continuous in t. We say that the pair of state and control trajectories $(x(t), u(t))$ is admissible, if when starting at x_0 the trajectories stay in $X \times U$ over $[0, T]$. The control functions that generate admissible trajectories are called admissible control functions.

Optimal control deals with the problem of finding a control law for a given system such that a certain optimality criterion is achieved. A control problem includes a cost functional that is a function of state and control variables. An optimal control is a set of differential equations describing the paths of the control variables that minimize the cost functional. The optimal control can be derived using Pontryagin's maximum principle (a necessary condition also known as Pontryagin's minimum principle or simply Pontryagin's Principle. The minimum cost function (also called performance function) is given by

$$J = \Phi[x(t_0), t_0, x(t_f), t_f] + \int_{t_0}^{t_f} L[x(t), u(t), t]dt \tag{2.7}$$

subject to first order dynamic constraints $\dot{x} = a[x(t), u(t), t]$, the algebraic path constraints $b[x(t), u(t), t] \leq 0$, and the boundary conditions $\phi[x(t_0), t_0, x(t_f), t_f] = 0$. The terms Φ and L are called the endpoint cost and Lagrangian, respectively. Thus, it is most often the case that any solution $[\mathbf{x}^*(t^*), \mathbf{u}^*(t^*), t^*]$ to the optimal control problem is locally minimizing.

2.2.1 Linear Quadratic Control, LQR

A special case of the general nonlinear optimal control problem given in the previous section is the linear quadratic (LQ) optimal control problem. The LQ problem is stated as follows. Minimize the quadratic continuous-time cost functional

$$J = \tfrac{1}{2}\mathbf{x}^{\mathrm{T}}(t_f)\mathbf{S}_f\mathbf{x}(t_f) + \tfrac{1}{2}\int_{t_0}^{t_f}[\,\mathbf{x}^{\mathrm{T}}(t)\mathbf{Q}(t)\mathbf{x}(t) + \mathbf{u}^{\mathrm{T}}(t)\mathbf{R}(t)\mathbf{u}(t)\,]\,\mathrm{d}\,t \tag{2.8}$$

Subject to the linear first-order dynamic constraints $\dot{\mathbf{x}}(t) = \mathbf{A}(t)\mathbf{x}(t) + \mathbf{B}(t)\mathbf{u}(t)$, and the initial condition $\mathbf{x}(t_0) = \mathbf{x}_0$

A particular form of the LQ problem that arises in many control system problems is that of the linear quadratic regulator (LQR) where all of the matrices (i.e, $\mathbf{A}, \mathbf{B}, \mathbf{Q}$ and $\mathbf{R}$) are constant, the initial time is arbitrarily set to zero, and the terminal time is taken in the limit $t_f \to \infty$(this last assumption is what is known as infinite horizon). The LQR problem is stated as follows. Minimize the infinite horizon quadratic continuous-time cost functional

$$J = \tfrac{1}{2}\int_{0}^{\infty}[\,\mathbf{x}^{\mathrm{T}}(t)\mathbf{Q}\mathbf{x}(t) + \mathbf{u}^{\mathrm{T}}(t)\mathbf{R}\mathbf{u}(t)\,]\,\mathrm{d}\,t \tag{2.9}$$

Subject to the linear time-invariant first-order dynamic constraints $\dot{\mathbf{x}}(t) = \mathbf{A}\mathbf{x}(t) + \mathbf{B}\mathbf{u}(t)$, and the initial condition $\mathbf{x}(t_0) = \mathbf{x}_0$.

In the finite-horizon case the matrices are restricted in that $\mathbf{Q}$ and $\mathbf{R}$ are positive semi-definite and positive definite, respectively. In the infinite-horizon case, however, the matrices $\mathbf{Q}$ and $\mathbf{R}$ are not only positive-semidefinite and positive-definite, respectively, but are also constant. These additional restrictions on $\mathbf{Q}$ and $\mathbf{R}$ in the infinite-horizon case are enforced to ensure that the cost functional remains positive. Furthermore, in order to ensure that the cost function is bounded, the additional restriction is imposed that the pair $(\mathbf{A}, \mathbf{B})$ is controllable. Note that the LQ or LQR cost functional can be thought of physically as attempting to minimize the control energy (measured as a quadratic form).
in classical optimal control theory that the LQ (or LQR) optimal control has the

feedback form

$$\mathbf{u}(t) = -\mathbf{K}(t)\mathbf{x}(t) \tag{2.10}$$

where $\mathbf{K}(t)$ is a properly dimensioned matrix, given as

$$\mathbf{K}(t) = \mathbf{R}^{-1}\mathbf{B}^{\mathrm{T}}\mathbf{S}(t), \tag{2.11}$$

and $\mathbf{S}(t)$ is the solution of the differential Riccati equation. The differential Riccati equation is given as

$$\dot{\mathbf{S}}(t) = -\mathbf{S}(t)\mathbf{A} - \mathbf{A}^{\mathrm{T}}\mathbf{S}(t) + \mathbf{S}(t)\mathbf{B}\mathbf{R}^{-1}\mathbf{B}^{\mathrm{T}}\mathbf{S}(t) - \mathbf{Q} \tag{2.12}$$

For the finite horizon LQ problem, the Riccati equation is integrated backward in time using the terminal boundary condition $\mathbf{S}(t_f) = \mathbf{S}_f$ For the infinite horizon LQR problem, the differential Riccati equation is replaced with the algebraic Riccati equation (ARE) given as

$$\mathbf{0} = -\mathbf{S}\mathbf{A} - \mathbf{A}^{\mathrm{T}}\mathbf{S} + \mathbf{S}\mathbf{B}\mathbf{R}^{-1}\mathbf{B}^{\mathrm{T}}\mathbf{S} - \mathbf{Q} \tag{2.13}$$

The matrices $\mathbf{A}, \mathbf{B}, \mathbf{Q}$, and $\mathbf{R}$ are all constant. In general multiple solutions to the algebraic Riccati equation and the positive definite (or positive semi-definite) solution is the one that is used to compute the feedback gain [26].

2.2.2 Kalman Filtering

The Kalman filter, also known as linear quadratic estimation (LQE), is an algorithm that uses a series of measurements observed over time, containing noise (random variations) and other inaccuracies, and produces estimates of unknown variables that tend to be more precise than those based on a single measurement alone. The algorithm works in a two-step process. In the prediction step, the Kalman filter produces estimates of the current state variables, along with their uncertainties. Once the outcome of the next measurement is observed, these estimates are updated using a weighted average, with more weight being given

to estimates with higher certainty. Because of the algorithm's recursive nature, it can run in real time using only the present input measurements and the previously calculated state; no additional past information is required.

The Kalman filter uses a system's dynamics model, known control inputs to that system, and multiple sequential measurements (such as from sensors) to form an estimate of the system's varying quantities (its state) that is better than the estimate obtained by using any one measurement alone. Details of the Kalman Filtering can be found in [24] [26].

2.2.2.1 Kalman Gain Derivation

The Kalman filter is a minimum mean-square error estimator. The error in the a posteriori state estimation is

$$\mathbf{x}_k - \hat{\mathbf{x}}_{k|k} \tag{2.14}$$

It is required to minimize the expected value of the square of the magnitude of this vector, $\mathrm{E}[|\mathbf{x}_k - \hat{\mathbf{x}}_{k|k}|^2]$. This is equivalent to minimizing the trace of the a posteriori estimate covariance matrix $\mathbf{P}_{k|k}$. By expanding out the terms in the equation above and collecting, it becomes

$$\mathbf{P}_{k|k} = \mathbf{P}_{k|k-1} - \mathbf{K}_k\mathbf{H}_k\mathbf{P}_{k|k-1} - \mathbf{P}_{k|k-1}\mathbf{H}_k^{\mathrm{T}}\mathbf{K}_k^{\mathrm{T}} + \mathbf{K}_k(\mathbf{H}_k\mathbf{P}_{k|k-1}\mathbf{H}_k^{\mathrm{T}} + \mathbf{R}_k)\mathbf{K}_k^{\mathrm{T}} \tag{2.15}$$

$$\mathbf{P}_{k|k} = \mathbf{P}_{k|k-1} - \mathbf{K}_k\mathbf{H}_k\mathbf{P}_{k|k-1} - \mathbf{P}_{k|k-1}\mathbf{H}_k^{\mathrm{T}}\mathbf{K}_k^{\mathrm{T}} + \mathbf{K}_k\mathbf{S}_k\mathbf{K}_k^{\mathrm{T}} \tag{2.16}$$

The trace is minimized when its matrix derivative with respect to the gain matrix is zero. Using the gradient matrix rules and the symmetry of the matrices involved it can be found that

$$\frac{\partial\, \mathrm{tr}(\mathbf{P}_{k|k})}{\partial\, \mathbf{K}_k} = -2(\mathbf{H}_k\mathbf{P}_{k|k-1})^{\mathrm{T}} + 2\mathbf{K}_k\mathbf{S}_k = 0. \tag{2.17}$$

Solving this for K_k yields the Kalman gain:

$$\mathbf{K}_k\mathbf{S}_k = (\mathbf{H}_k\mathbf{P}_{k|k-1})^{\mathrm{T}} = \mathbf{P}_{k|k-1}\mathbf{H}_k^{\mathrm{T}} \tag{2.18}$$

$$\mathbf{K}_k = \mathbf{P}_{k|k-1}\mathbf{H}_k^{\mathrm{T}}\mathbf{S}_k^{-1} \tag{2.19}$$

This gain is known as the optimal Kalman gain.

2.2.3 $\mathcal{H}_2$ and $\mathcal{H}_\infty$

$\mathcal{H}_\infty$ methods are used in control theory to synthesize controllers achieving stabilization with guaranteed performance. $\mathcal{H}_\infty$ is expressed mathematical optimization problem which is then used to find the optimal controller. $\mathcal{H}_\infty$ techniques have the advantage over classical control techniques in that they are readily applicable to problems involving multivariable systems with cross-coupling between channels. The resulting controller is only optimal with respect to the prescribed cost function and does not necessarily represent the best controller in terms of the usual performance measures used to evaluate controllers such as settling time, energy expended, etc.

$\mathcal{H}_\infty$ is the space of matrix-valued functions that are analytic and bounded in the open right-half of the complex plane defined by $Re(s) > 0$; the $\mathcal{H}_\infty$ norm is the maximum singular value of the function over that space. This can be interpreted as a maximum gain in any direction and at any frequency; for SISO systems, this is effectively the maximum magnitude of the frequency response. $\mathcal{H}_\infty$ techniques can be used to minimize the closed loop impact of a perturbation: depending on the problem formulation, the impact will either be measured in terms of stabilization or performance. The process is represented according to the following standard configuration as shown in Figure 2.2.

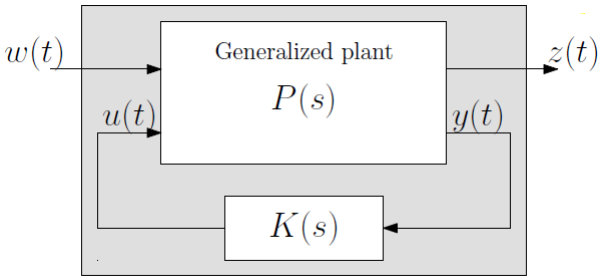

FIGURE 2.2: Generalised Plant Model.

The plant $P(s)$ has two inputs, the exogenous input $w(t)$, that includes reference signal and disturbances, and the manipulated variables $u(t)$. There are two outputs, the error signals $z(t)$ that is required to minimize, and the measured variables $y(t)$, that we use to control the system. $y(t)$ is used in $K(s)$ to calculate the manipulated variable $u(t)$. Notice that all these are generally vectors, whereas $P(s)$ and $K(s)$ are matrices. In formulae, the system is:

$$\begin{bmatrix} z \\ v \end{bmatrix} = \mathbf{P}(s) \begin{bmatrix} w \\ u \end{bmatrix} = \begin{bmatrix} P_{11}(s) & P_{12}(s) \\ P_{21}(s) & P_{22}(s) \end{bmatrix} \begin{bmatrix} w \\ u \end{bmatrix} \tag{2.20}$$

$$u = \mathbf{K}(s)\, y \tag{2.21}$$

It is therefore possible to express the dependency of z on w as:

$$z = F_\ell(\mathbf{P}, \mathbf{K})\, w \tag{2.22}$$

Called the lower linear fractional transformation, F_ℓ is defined (the subscript comes from lower):

$$F_\ell(\mathbf{P}, \mathbf{K}) = P_{11} + P_{12}\, \mathbf{K}\, (I - P_{22}\, \mathbf{K})^{-1}\, P_{21} \tag{2.23}$$

Therefore, the objective of $\mathcal{H}_\infty$ control design is to find a controller $\mathbf{K}$ such that $F_\ell(\mathbf{P}, \mathbf{K})$ is minimised according to the $\mathcal{H}_\infty$ norm. The same definition applies to $\mathcal{H}_2$ control design. The infinity norm of the transfer function matrix $F_\ell(\mathbf{P}, \mathbf{K})$ is defined as:

$$||F_\ell(\mathbf{P}, \mathbf{K})||_\infty = \sup_\omega \bar{\sigma}(F_\ell(\mathbf{P}, \mathbf{K})(j\omega)) \tag{2.24}$$

where $\bar{\sigma}$ is the maximum singular value of the matrix $F_\ell(\mathbf{P}, \mathbf{K})(j\omega)$. The achievable $\mathcal{H}_\infty$ norm of the closed loop system is mainly given through the matrix D_11 (when the system P is given in the form $(A, B_1, B_2, C_1, C_2, D_{11}, D_{12}, D_{22}, D_{21})$ [3][26].

2.3 Aircraft Model Generation

The aircraft model used for loads analysis and design and validation of the GLAS is based on aerodynamic and structural data of the BWB configuration NACRE-FW1 developed in the European project NACRE [4] Figure 2.3 illustrates the geometry of the NACRE-FW1

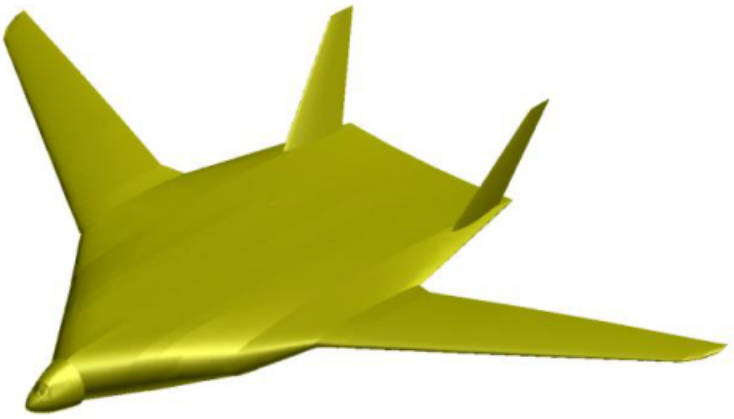

FIGURE 2.3: Geometry without engines of the NACRE-FW1 Configuration. [4].

The original model of the primary structure of the NACRE-FW1 configuration was not designed for dynamic analysis. Necessary modifications and extensions were required which comprise integration of additional structural elements for improved stiffness. Components like cockpit, elevators, rudders, wing's leading and trailing edges, landing gears, as well as engine and pylon structure were replaced by concentrated masses, see Figure 2.4.

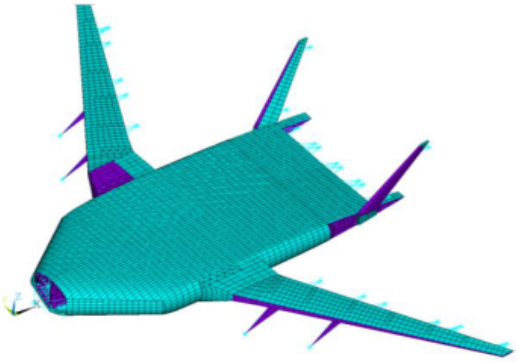

FIGURE 2.4: Modified and extended finite element model of the NACRE-FW1 configuration [4].

Non-structural masses of systems and equipment as well as operational masses (as defined in the NACRE project) were integrated into the structural model. Finally, various passenger/payload and fuel configurations were modelled with concentrated masses and also integrated into the structural model of the NACRE-FW1 configuration, see Figure 2.5. Such prepared sets of structural models were reduced to the first 100 structural Eigen modes [**?**].

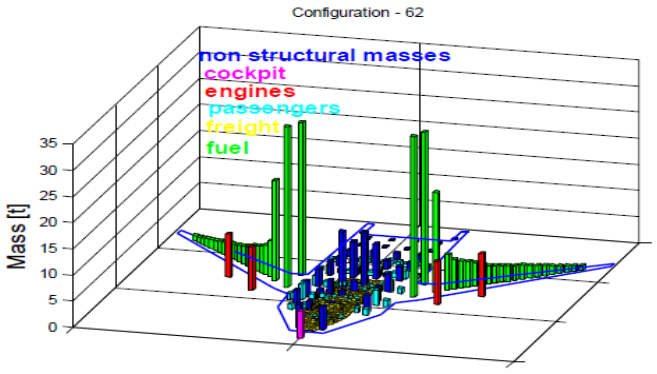

FIGURE 2.5: Scheme of non-structural masses [4].

Fuel mass configurations are set up in order to stay within the centre of gravity (CG) range defined in the NACRE project. Aerodynamic polars, damping derivatives, and control surface derivatives were provided by the NACRE project for various low and high speed cases. The used analysis methods range from surface panel methods to CFD. The control surfaces of the investigated BWB airliner are illustrated in Figure 2.6.

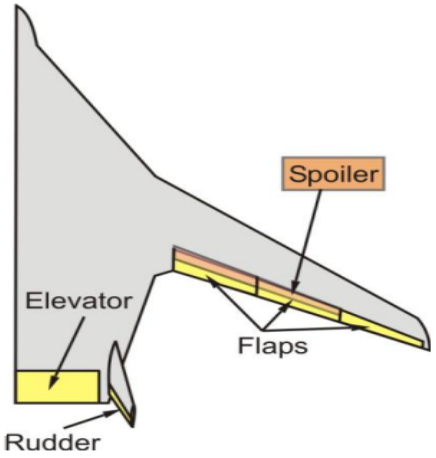

FIGURE 2.6: BWB control surface setting [4].

2.4 Gust Modelling

Vertical gust were modelled as a function of $(1 - \cos\theta)$. Worst case scenario was considered, and it was assumed that the worst scenarios takes place at a fastest gust speed of $19m/s$. Various gust lengths were considered as shown in the Figure 2.7 The main problems were with the shorter gust lengths, since the actuator and the sensors were not fast enough to react to the shorter gusts. Therefore emphasis was given on shorter gust lengths, which was defined as the worst case scenario.

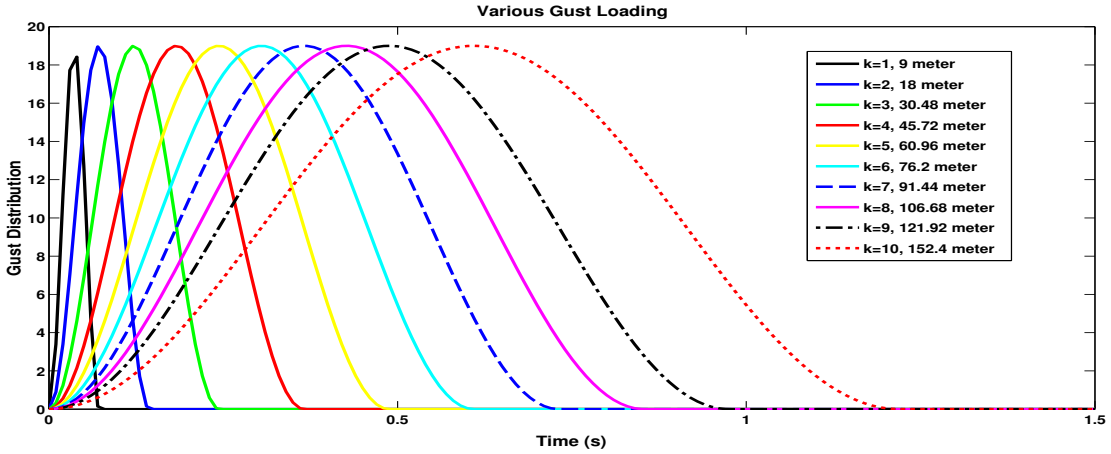

FIGURE 2.7: Gust distribution of various gust lengths.

No. of Cases	**Gust Length (m)**
k = 1	9
k = 2	18
k = 3	30.48
k = 4	45.72
k = 5	60.96
k = 6	76.2
k = 7	91.44
k = 8	106.68
k = 9	121.92
k = 10	152.4

TABLE 2.1: Different gust cases.

Chapter 3

Validation

The first part of the thesis work involved validating the non-linear Simulink model provided by the ACFA 2020 project with linear MATLAB model. This was required to eliminate the non-linearities in actuator's Simulink model such as rate-limiters, saturation points. The validation was intended to check that the linear MATLAB model exactly matches the non-linear Simulink model.

3.1 Actuators

Reasonable control system delays are taken into account by $2nd$ order Pade filters. The actuators are modelled as nonlinear subsystems taking into account that the achievable actuator deflection rate is a function of the aerodynamic forces acting on the control surface and thus a function of the deflection angle. Actuators models are considered as 2nd order linear models augmented by saturations and rate limiters [17]. There were mainly 7 control actuators for the aircraft, namely 1) Three Flaps 2) Elevator 3) Spoiler 4) Mini flap and 5) Rudder.

3.1.1 Elevator and Spoiler Model

The non-linear elevator and spoiler model depended on hydraulic pressure and hinge moment. The non-linear architecture of these two actuator is presented in the Figure 3.1.

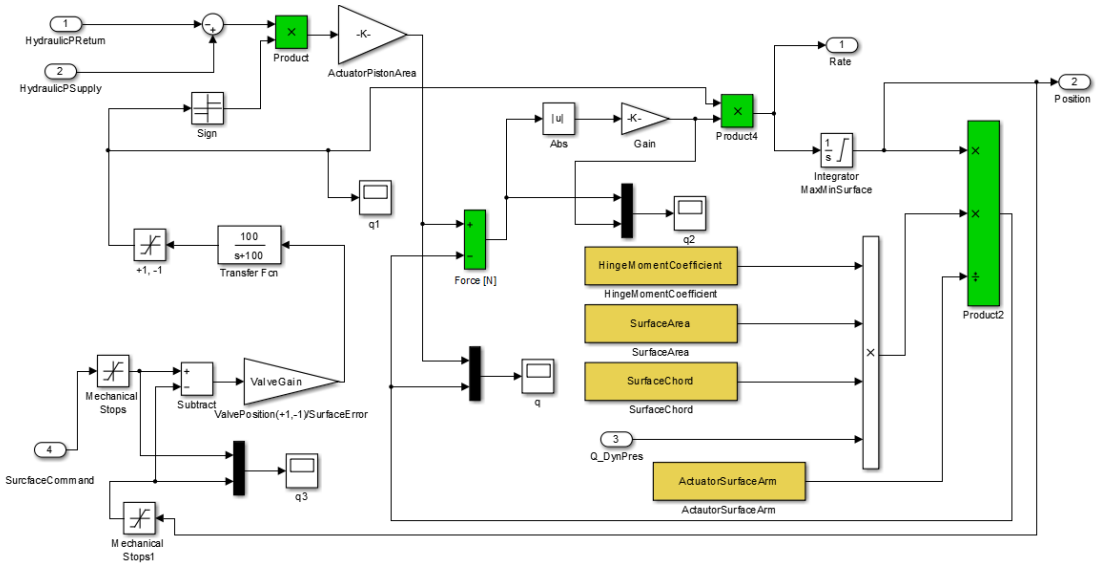

FIGURE 3.1: Non-linear Elevator and Spoiler Model.

The non-linear model was approximated by state-space description with one input and two output.

$$\dot{x} = \begin{bmatrix} 0 & -100 \\ 1 & -20 \end{bmatrix} \begin{pmatrix} x_1 \\ x_2 \end{pmatrix} + \begin{bmatrix} 100 \\ 0 \end{bmatrix} \delta_e \tag{3.1}$$

$$y = \begin{bmatrix} 0 & 1 \\ 1 & -20 \end{bmatrix} \begin{pmatrix} x_1 \\ x_2 \end{pmatrix} \tag{3.2}$$

where the input is the actuator deflection and the outputs are deflection and deflection rate.

Similarly Rudders, Flaps and Mini flaps were approximated by the state-space description in equation 3.3 - 3.8, for Flaps

$$\dot{x} = \begin{bmatrix} 0 & -1600 \\ 1 & -80 \end{bmatrix} \begin{pmatrix} x_1 \\ x_2 \end{pmatrix} + \begin{bmatrix} 1600 \\ 0 \end{bmatrix} \delta_e \tag{3.3}$$

$$y = \begin{bmatrix} 0 & 1 \\ 1 & -80 \end{bmatrix} \begin{pmatrix} x_1 \\ x_2 \end{pmatrix} \tag{3.4}$$

For MiniFlap

$$\dot{x} = \begin{bmatrix} 1000 & -14409 \\ 1 & -720 \end{bmatrix} \begin{pmatrix} x_1 \\ x_2 \end{pmatrix} + \begin{bmatrix} 14409 \\ 0 \end{bmatrix} \delta_{MF} \tag{3.5}$$

$$y = \begin{bmatrix} 0 & 1 \\ 1 & -720.4611 \end{bmatrix} \begin{pmatrix} x_1 \\ x_2 \end{pmatrix} \tag{3.6}$$

For Rudder

$$\dot{x} = \begin{bmatrix} 0 & -100 \\ 1 & -20 \end{bmatrix} \begin{pmatrix} x_1 \\ x_2 \end{pmatrix} + \begin{bmatrix} 100 \\ 0 \end{bmatrix} \delta_{RU} \tag{3.7}$$

$$y = \begin{bmatrix} 0 & 1 \\ 1 & -20 \end{bmatrix} \begin{pmatrix} x_1 \\ x_2 \end{pmatrix} \tag{3.8}$$

3.2 Sensor Delay Approximation

Sensors are subject to a time delay due to signal processing latency, modeled via a 2nd order Pade approximation) and additionally low-pass filtered via Butterworth filters of 2nd order. 160ms time-delay uses $2nd$ order Pade approximation in which 40ms was accounted for computation and 20ms for sampling and 100ms for measurement delay. For 60ms time-delay, 40ms is accounted for computation and 20ms for sampling. Figure 3.2 shows the approximation in the Simulink model. The Butterworth filter has the transfer function as below

$$IRBW(s) = \frac{1}{0.00281s^2 + 0.075s + 1} \tag{3.9}$$

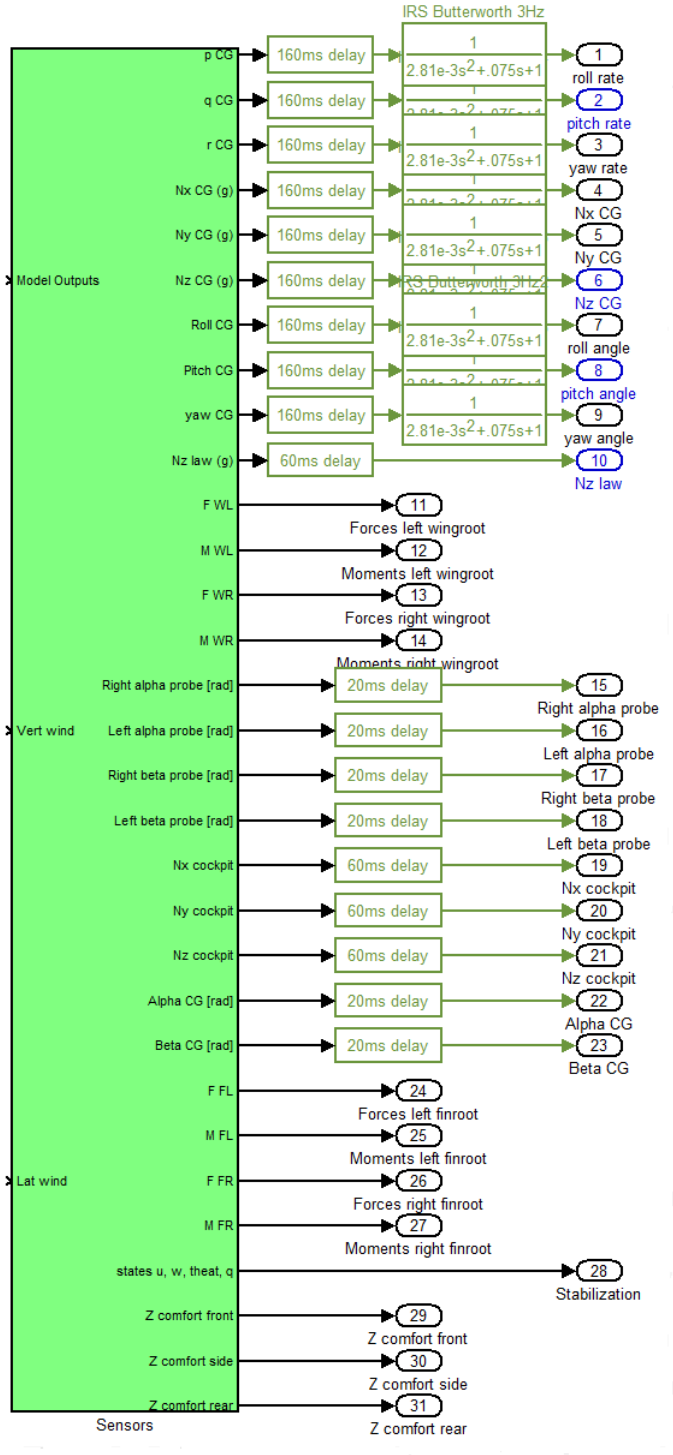

FIGURE 3.2: Delay approximations.

60ms Delay transfer function was approximated as below

$$Delay60ms(s) = \frac{s^2 - 100s + 3333}{s^2 + 100s + 3333} \tag{3.10}$$

160ms Delay was approximated by

$$Delay160ms(s) = \frac{s^2 - 37.5s + 468.8}{s^2 + 37.5s + 468.8} \tag{3.11}$$

160ms Delay after Butterworth filtering was approximated by

$$Delay160msIRWB(s) = \frac{s^2 - 37.5s + 468.8}{0.00281s^4 + 0.1804s^3 + 5.13s^2 + 72.66s + 468.8} \tag{3.12}$$

20ms Delay after Butterworth filtering was approximated by

$$Delay20ms(s) = \frac{s^2 - 300s + 30000}{s^2 + 300s + 30000} \tag{3.13}$$

3.3 Validation Plots

The Simulink Model provided by the industry and the simplified MATLAB model needed to validated. Both the models were validated by giving a step response to the input and look for the matching between the two responses.

For the validation, a simple *Step* input was given to the elevator 1 and the outputs from both the model were plotted.

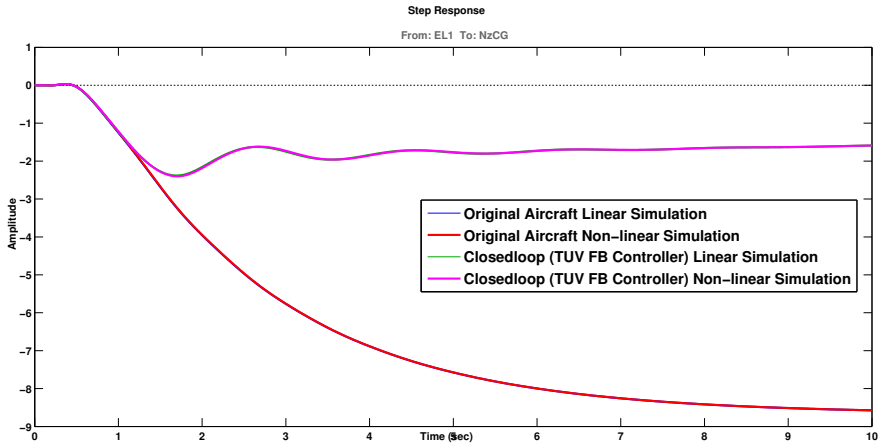

FIGURE 3.3: NzCG response to Elevator 1 step deflection.

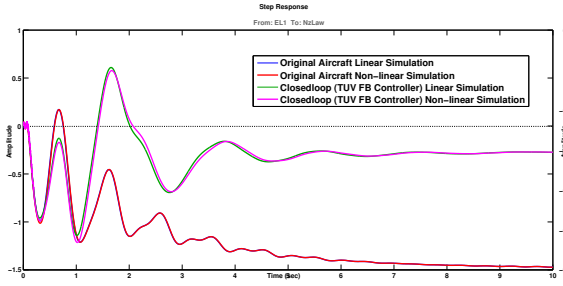

FIGURE 3.4: NzLaw response to Elevator 1 step deflection.

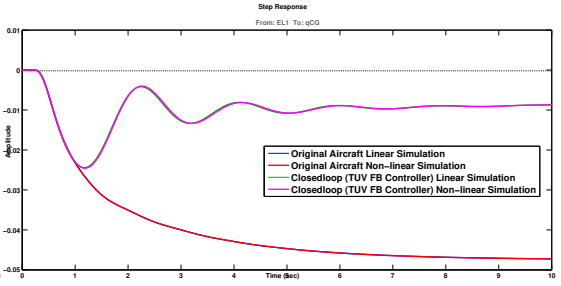

FIGURE 3.5: q_{CG} response to Elevator 1 step deflection.

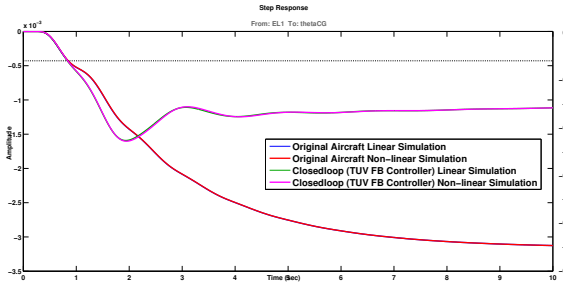

FIGURE 3.6: θ_{CG} response to Elevator 1 step deflection.

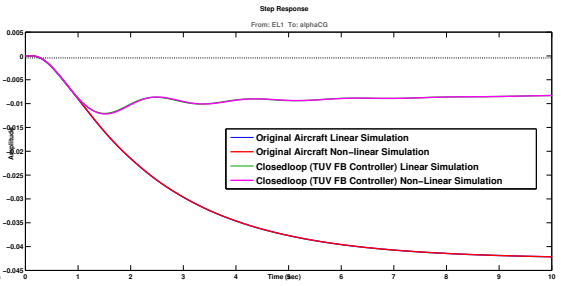

FIGURE 3.7: α_{CG} response to Elevator 1 step deflection.

From the plots in Figure 3.3-3.7 , it can be seen that the MATLAB model and Simulink models were matching closely. Hence the model connections and approximation were close and well approximated. It can also be seen that the original aircraft is unstable. The original aircraft is stabilized by the Feedback controller designed by TUV control group [12] [16] [19] (discussed in chapter 4.2).

Chapter 4

Design of New Controller

A well documented solution for the reduction of wing root bending due to gust loading is using feedback control in conjunction with feedforward control. The solution worked for nominal cases for example various gust lengths. Due to the time lag of the control surface and the computational delays it was only possible to improve the performance for the gusts bigger than $60.96m(k = 5)$. For the shorter gust lengths use of feedforward control action reduced the first wing bending but excited the 2nd and 3rd wing bending significantly. Therefore the new controller needed to improve the performance of the feedforward controller with respect to reducing the 2nd and 3rd wing bending for shorter gust lengths.

Figure 4.1 and 4.2 shows the primary control surface of the NACRE aircraft. It had three ailerons, two spoilers, one miniflap, two rudders and elevators. Flap 1 and Flap 2 is positioned right below the Spoiler 1 and 2. And the Flap 3 is placed at the outer most position. The primary function of the Flap 3 was to perform coordinated turn and control rolling moments. In addition the rudder had a "Twin-tail" configuration.

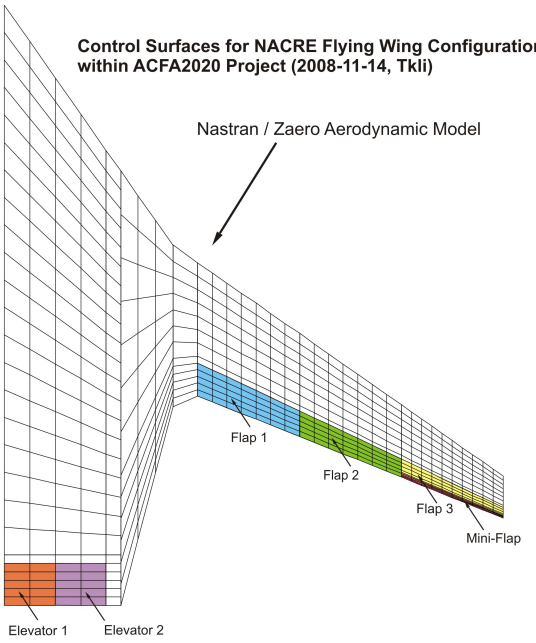

FIGURE 4.1: Primary control surfaces for the NACRE BWB aircraft.

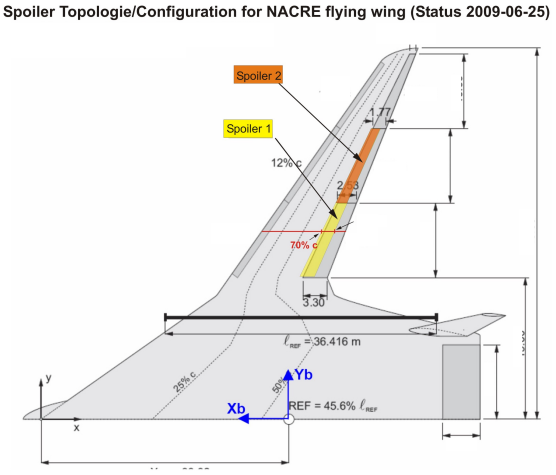

FIGURE 4.2: Spoiler Configuration for NACRE BWB aircraft.

A sequence of feedforward actions were calculated for gust loading which was same with respect to various mass cases, altitude, Mach numbers and any gust length [5]. The feedforward action involved using the Elevator and Spoilers. For the feedforward action, it was decided that the Elevator 1 and 2 will work together as one single elevator and the spoiler 1 and 2 will work together as one single spoiler. The feedforward control sequence is shown in Figure 4.3.

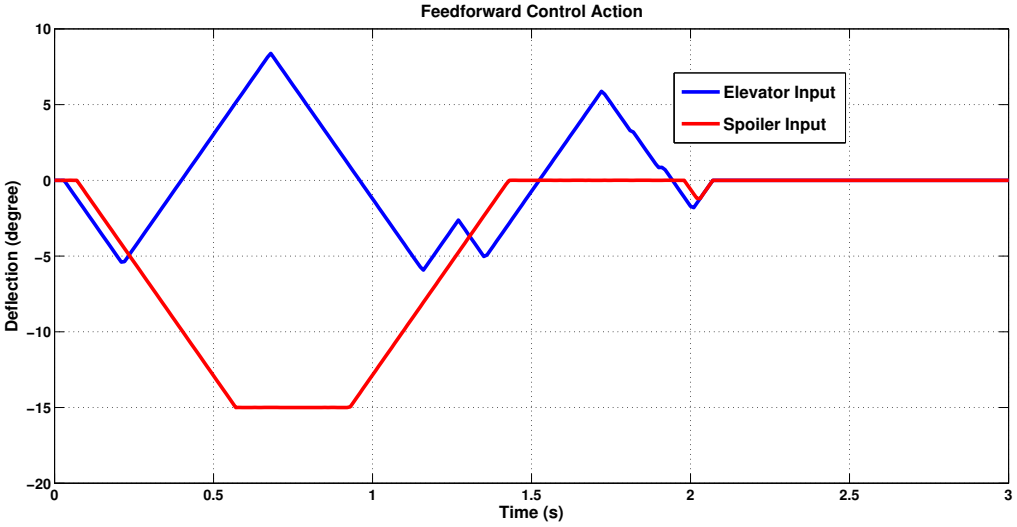

FIGURE 4.3: Feedforward Control Inputs [5].

The aim of the new controller was to design a new η_z controller which could work along with the feedforward controller improving its performance over shorter gust lengths. The newly designed controller also needed to be robust in terms of different mass cases and have improved performance in reduction of wing root moment in time domain.

For the validation of the new η_z controller 6 different mass cases and 10 gust lengths were chosen, in total 60 cases. Considering the worst case scenario the cruise speed of the aircraft 0.85 Mach (250 m/s) was made fixed at a cruising altitude of 12500 meter was chosen. Table 4.1 shows the mass variation of the NACRE aircraft.

No. of Cases	**Fuel (as a fraction of full load)**
1	1/16th
2	1/8th
3	1/4th
4	1/2nd
5	3/4th
6	1

TABLE 4.1: Mass variation cases.

4.1 η_z Law

The wing bending of the flexible aircraft was assessed by attaching sensors that would measure the r.m.s values of acceleration at a number of locations on the aircraft. For precisely determining the effects of wing bending the sensors were placed at the Centre of Gravity (CG), wingtip node right and wing tip node left. Details description for the placement of the sensors can be found in [27]. The sensors were place to measure the vertical acceleration (z-axis) at the defined locations. The acceleration of the wing relative to the centre of gravity is defined

as $\eta_z Law$, and it is calculated by:

$$\eta_z Law = \frac{1}{2}\eta_z wingtipnoderight + \frac{1}{2}\eta_z wingtipnodeleft - \eta_z CG \qquad (4.1)$$

4.2 Classical Loop by Loop SISO Design

The considered BWB airline was statically unstable in large regions of mass and flight envelope. Figure 4.4 shows the unstable pole-zero plot of the original aircraft. Therefore, the flight control system needed to provide artificial pitch stabilization [12]. Details of the flight control laws are outlined in [16] [19].

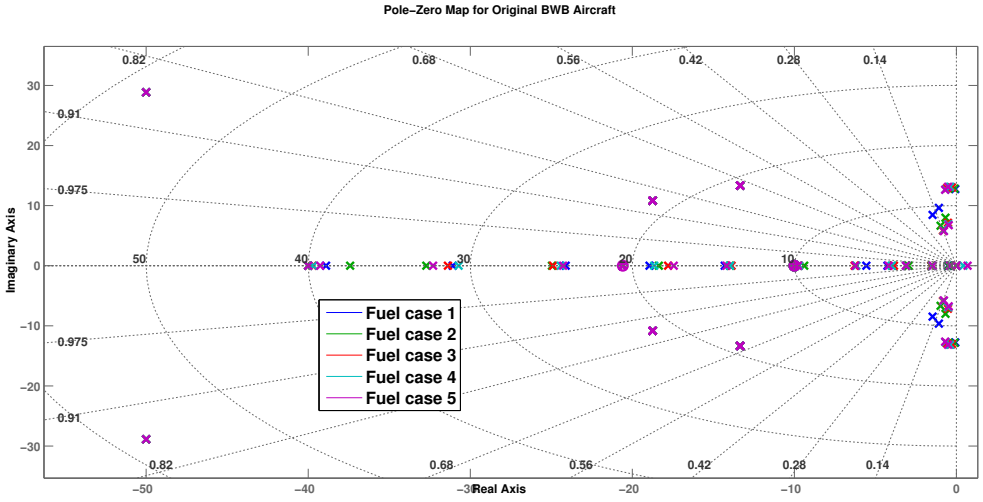

FIGURE 4.4: Pole-Zero plots of the original BWB aircraft.

The original model of the aircraft was stabilized by the feedback controller designed by TUV group. Artificial pitch stiffness is achieved by feedback of the vertical CG load factor η_z to the elevators. In order to achieve neutral pitch stability this feedback is done via a PI controller [4] [13] [14] [15]. An additional pitch damper (i.e. feedback from pitch rate q to the elevators) allows placement of the poles of the angle of attack mode. Figure 4.2 shows the control block diagram of the feedback controller. Designed feedback controller was robust with respect to mass/fuel cases. Figure 4.6 illustrates the closed loop pole zero placement for the different mass cases.

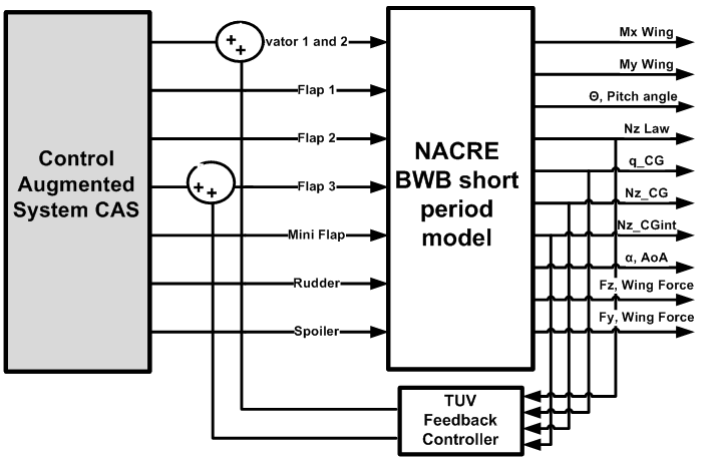

FIGURE 4.5: Stabilizing TUV Feedback Controller.

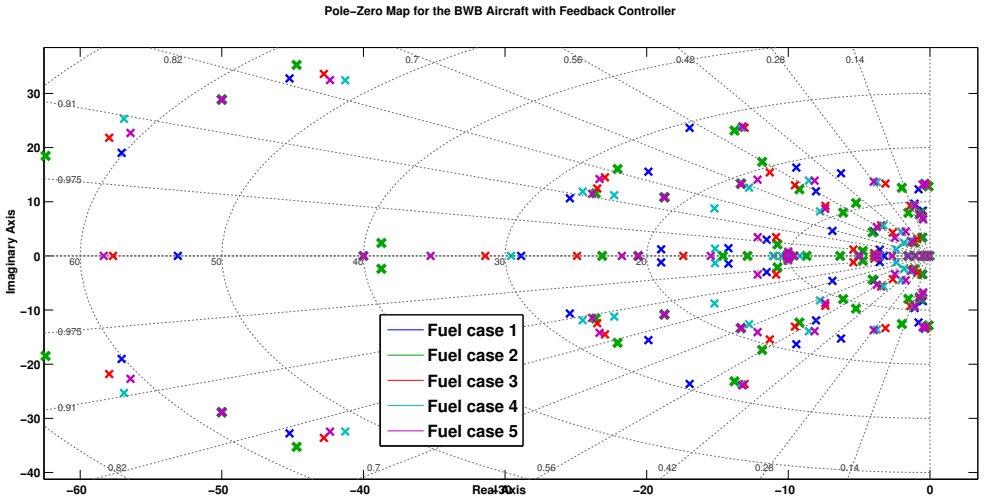

FIGURE 4.6: Pole-Zero plots of the BWB aircraft with Feedback Controller.

In case of a gust disturbance, the concept was to feedback the η_z Law to the flap 1 (inner aileron) and flap 2 (centre aileron), which would work together with the feedforward controller and the feedback controller designed by TUV group. Figure 4.7 shows the control block diagram for the new control strategy.

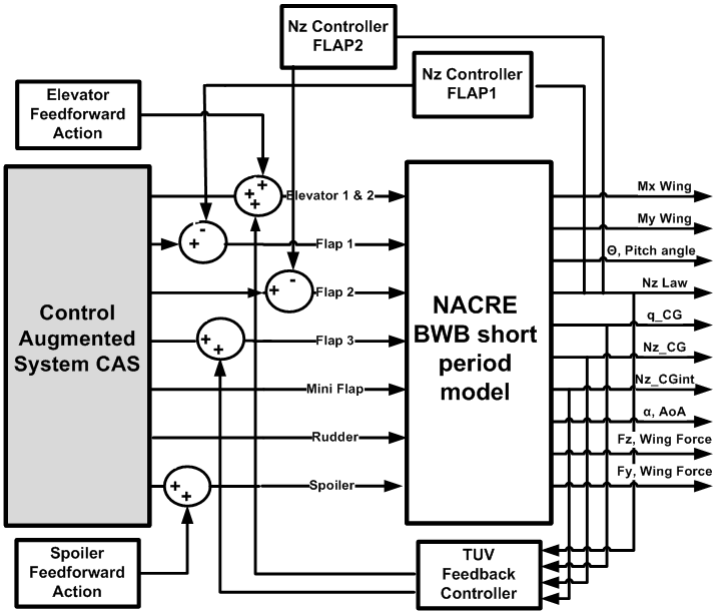

FIGURE 4.7: New SISO Control Strategy by Feeding η_z Law to Flap 1 and Flap 2.

4.2.1 η_z Controller Design to Flap 1

The first wind bending mode from η_z law to flap 1 (inner aileron) lied between $6 - 10Hz$. η_z controller was design using the root locus method. Equation 4.2 shows the transfer function of the designed η_z controller.

$$\eta_z LawtoFlap1 = \frac{6}{s^2 + 12s + 20} \tag{4.2}$$

In frequency domain the channel from Flap 1 to $\eta_z$law was already damped by 5-7dB by the TUV controller [**?**]. While designing the controller using root locus method it was ensured that the lower frequency of the aircraft is not excited. If the lower frequency is excited then it will lead the aircraft to unwanted oscillations [21] [22] [23] [25]. Figure 4.8 shows the bode diagram plot of the $\eta_z LawtoFlap1$ over different mass cases. The red line shows the frequency response using η_z, cyan line shows the stabilized aircraft and the green line shows the controller frequency response.

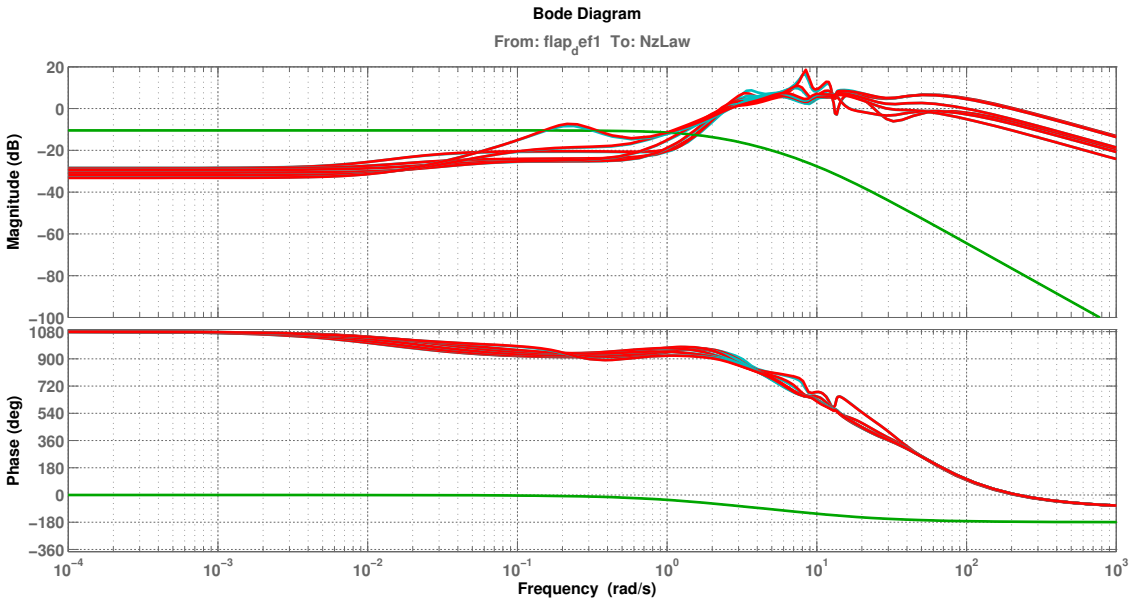

FIGURE 4.8: Bode plot for different mass cases (1 to 6) using $\eta_z LawtoFlap1$.

The designed η_z controller was a low pass filter with a cut-off frequency at 1 Hz. Bode plot ensures that the long period or the Phugiod mode of the aircraft was not excited.

4.2.2 η_z Controller Design to Flap 2

The first wind bending mode from η_z law to flap 2 (centre aileron) lied between $2-3Hz$. η_z controller was design using the root locus method. Equation 4.3 shows the transfer function of the designed η_z controller.

$$\eta_z LawtoFlap2 = \frac{0.1s+1}{s+1} \tag{4.3}$$

Similar strategies as Flap 1 was also used to design the η_z controller to Flap 2. It was ensured that the long period (low frequency) region of the aircraft is not excited. The Figure 4.9 shows the bode plot of the η_z controller over different mass cases. The designed filter was a first order filter with one zero and one pole.

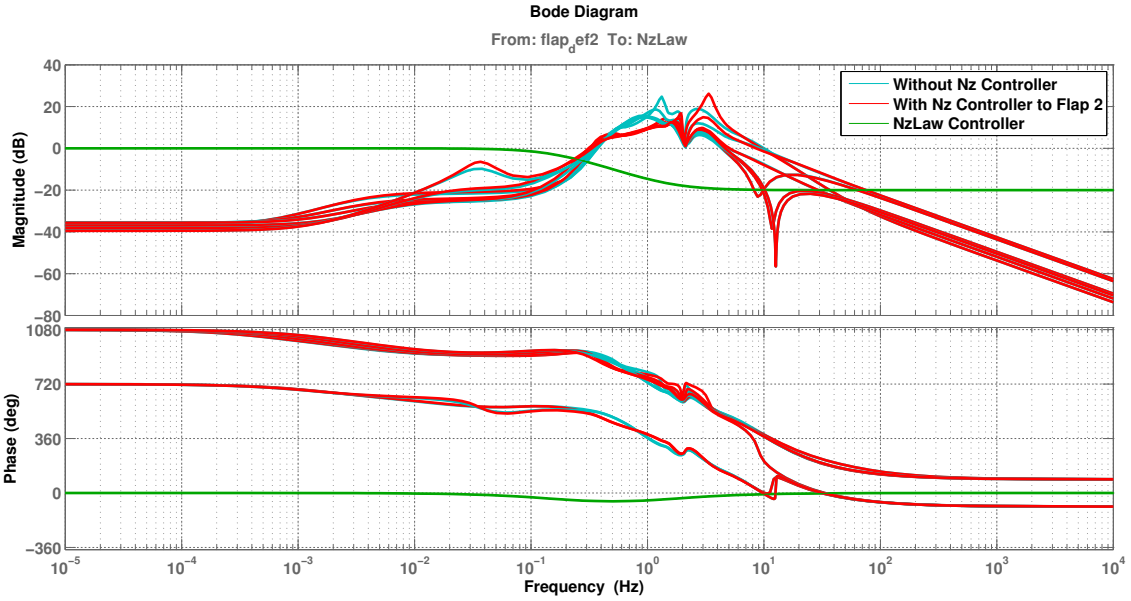

FIGURE 4.9: Bode plot for different mass cases for (1 to 6) using $\eta_z LawtoFlap2$.

4.2.3 Performance Comparison Over Different Gust Lengths using SISO design

Different mass cases (6 mass cases) were varied along with the gust lengths (10 gust lengths). The rate limiters and the saturation point of the Flap 1 and 2 were also taken into account during the simulation. Flap 1 and Flap 2 was constrained by a rate limiter at $\pm 40 deg/sec$ and saturation point at $\pm 25^o$. M_x is defined as the wing root bending moment and M_y is defined as the wing root torsional moment. Figure 4.10 to 4.19 shows the response of the wing root moments M_x and M_y for the gust cases k=1, 2, 5, 9, 10. All other gust cases had similar responses. The cyan line corresponds to the original aircraft with TUV Feedback controller, blue line corresponds to aircraft with feedforward action and the red line corresponds to the aircraft with feedforward controller plus newly designed $\eta_z Law$ controller to flap 1 and 2.

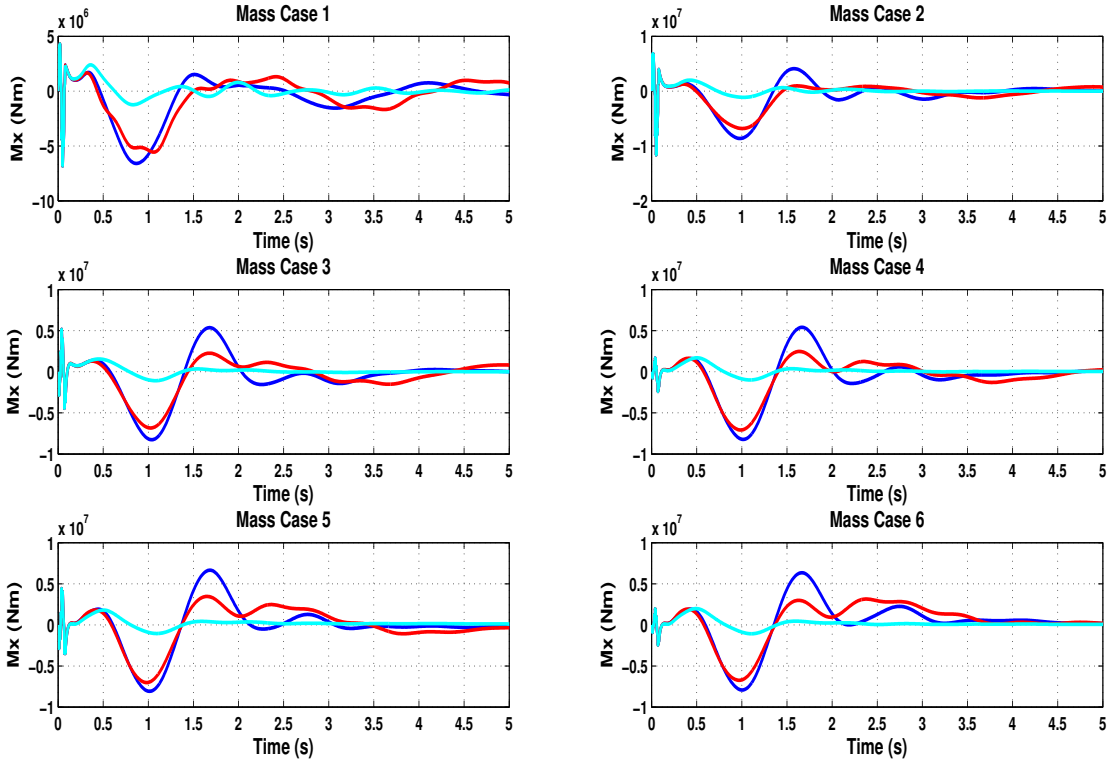

FIGURE 4.10: Wing Root Moment, M_x at gust length 9m (k=1) for different mass cases using SISO controller.

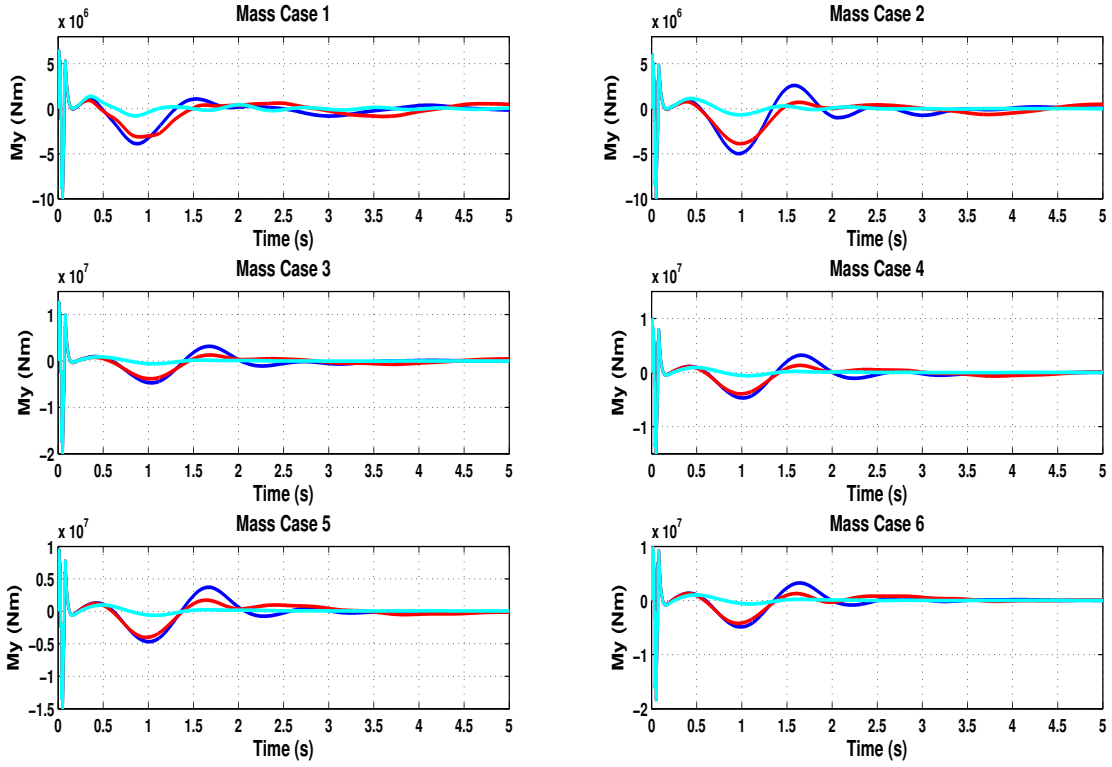

FIGURE 4.11: Wing Root Moment, M_y at gust length 9m (k=1) for different mass cases using SISO controller.

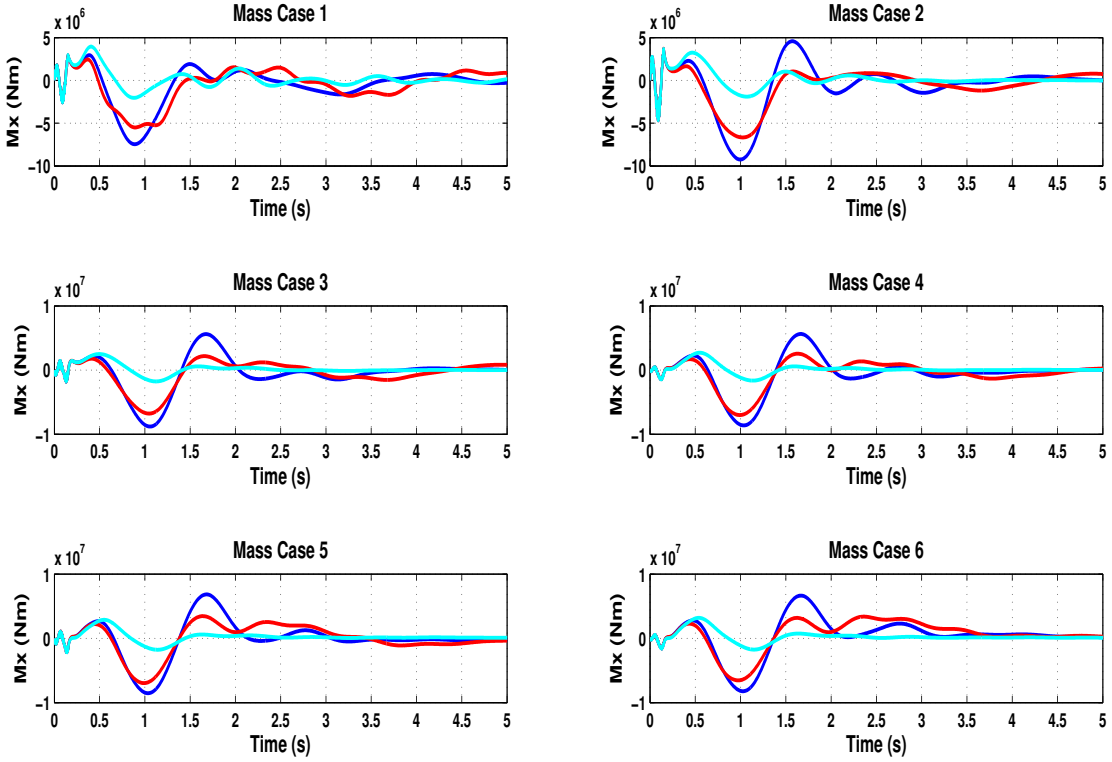

FIGURE 4.12: Wing Root Moment, M_x at gust length 18m (k=2) for different mass cases using SISO controller.

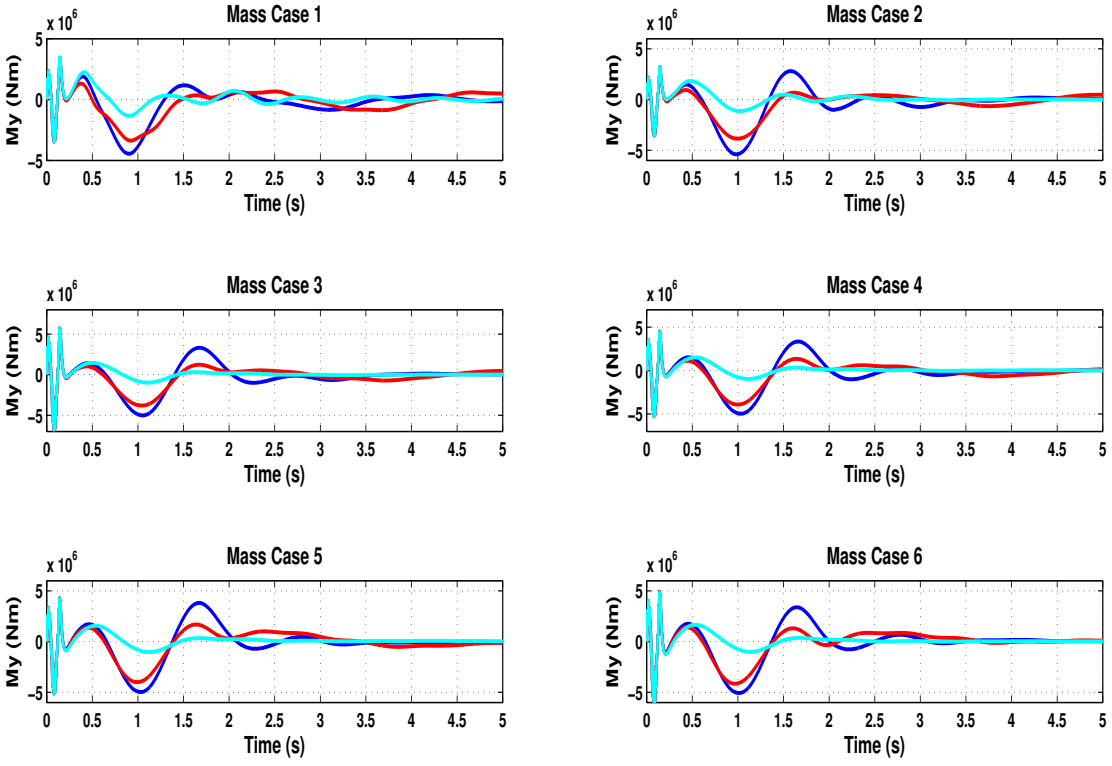

FIGURE 4.13: Wing Root Moment, M_y at gust length 18m (k=2) for different mass cases using SISO controller.

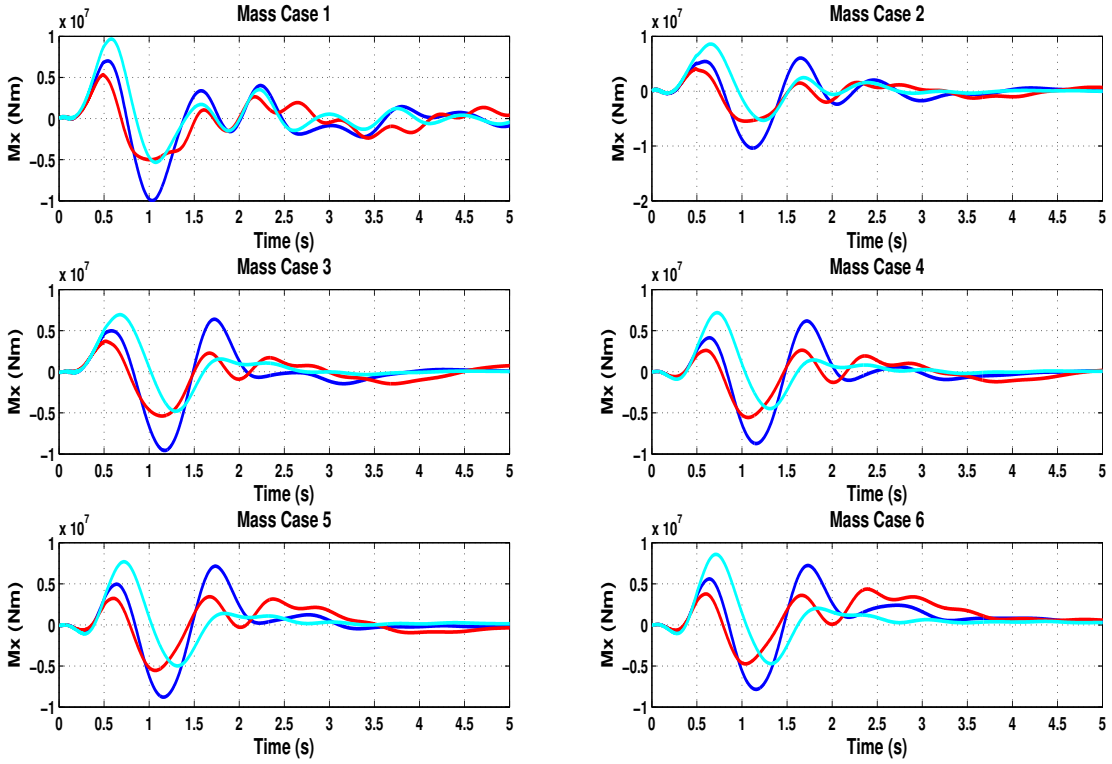

FIGURE 4.14: Wing Root Moment, M_x at gust length 60.96m (k=5) for different mass cases using SISO controller.

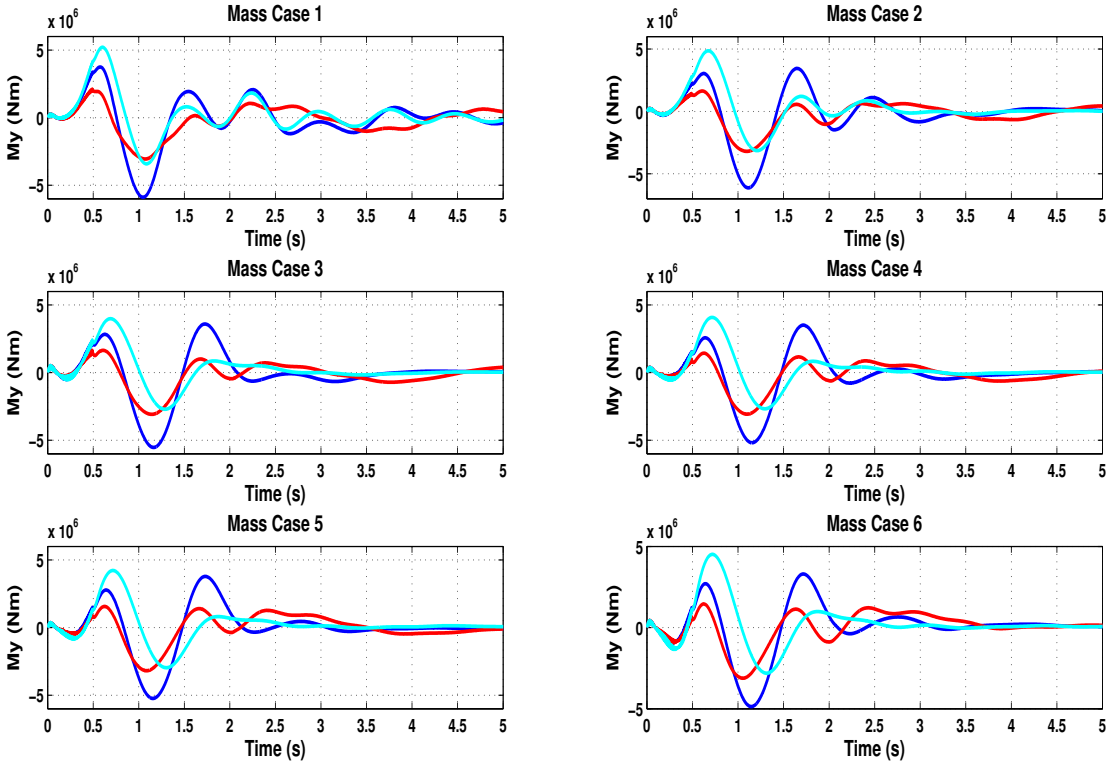

FIGURE 4.15: Wing Root Moment, M_y at gust length 60.96m (k=5) for different mass cases using SISO controller.

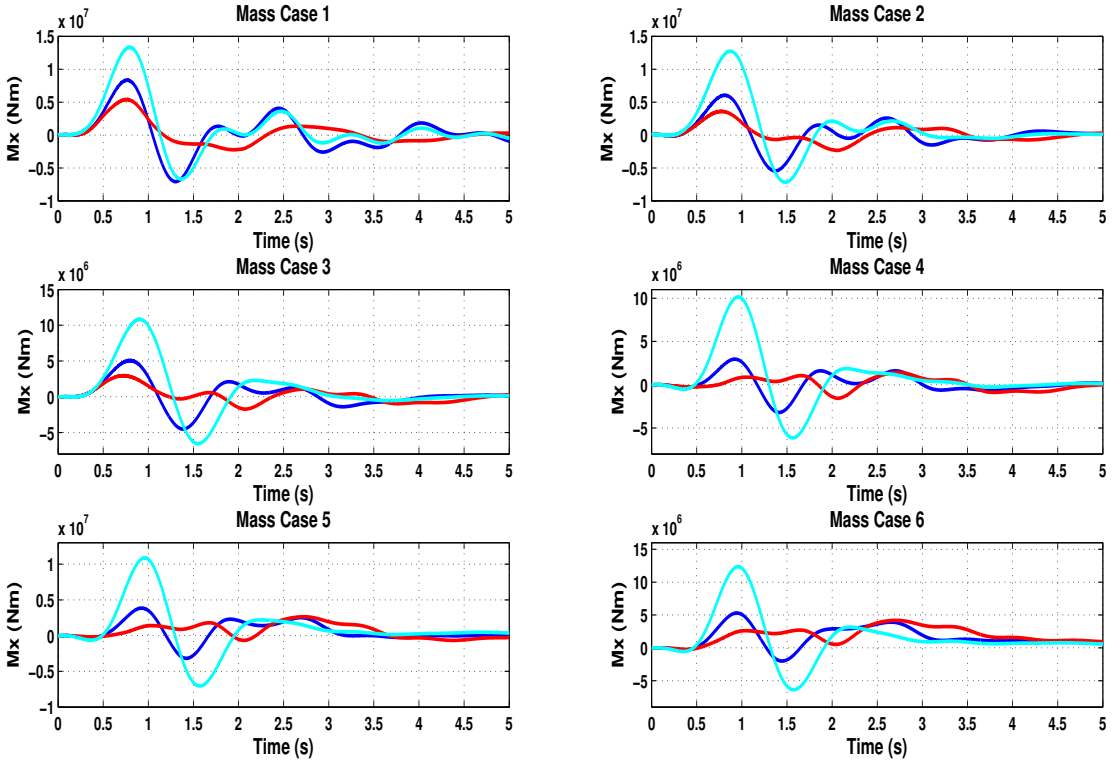

FIGURE 4.16: Wing Root Moment, M_x at gust length 121.92m (k=9) for different mass cases using SISO controller.

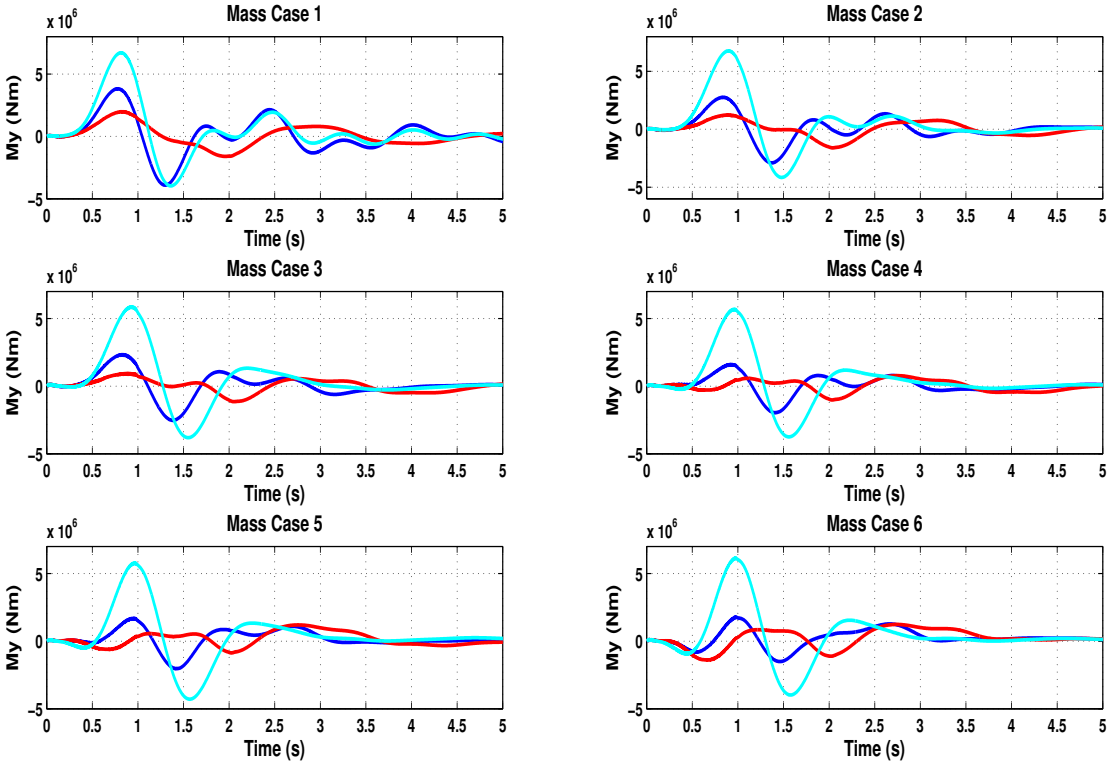

FIGURE 4.17: Wing Root Moment, M_y at gust length 121.92m (k=9) for different mass cases using SISO controller.

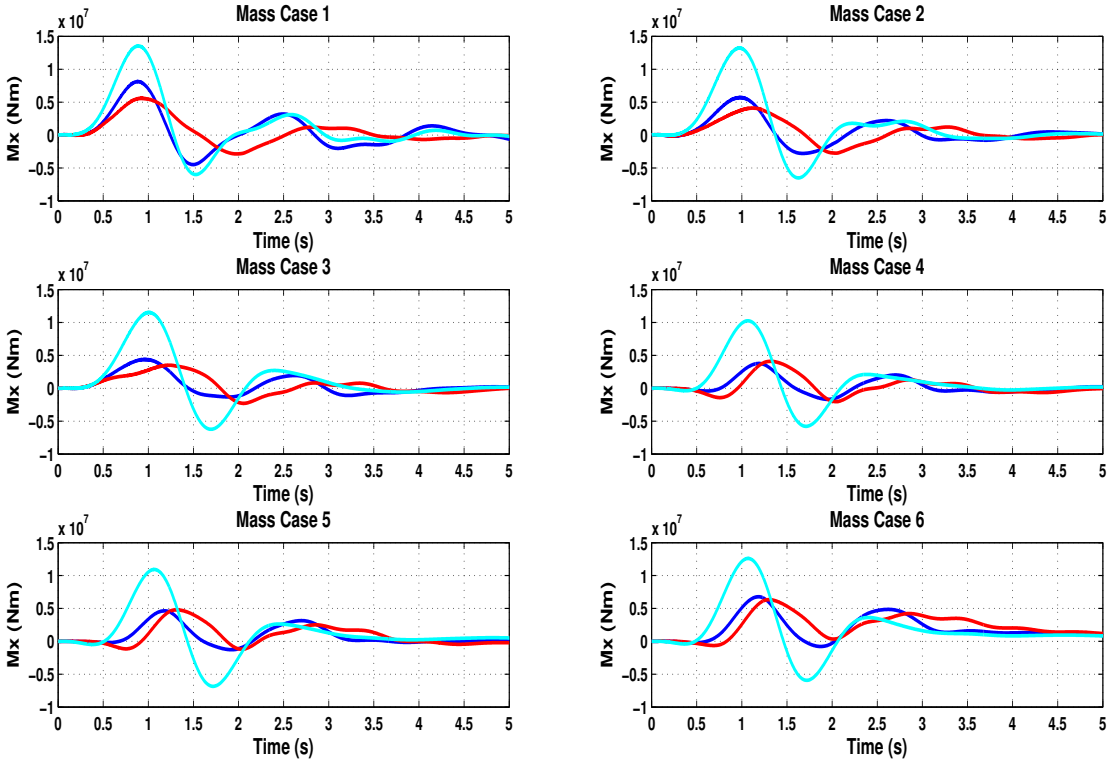

FIGURE 4.18: Wing Root Moment, M_x at gust length 152.4m (k=10) for different mass cases using SISO controller.

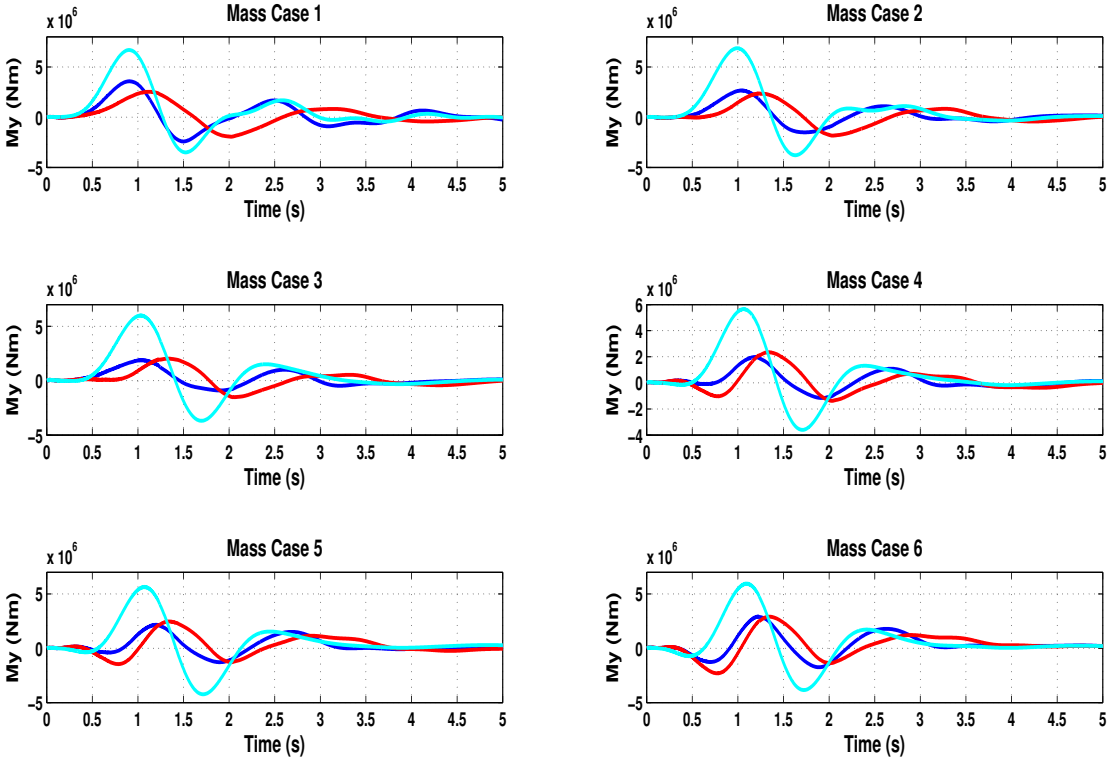

FIGURE 4.19: Wing Root Moment, M_y at gust length 152.4m (k=10) for different mass cases using SISO controller.

The reductions in the peaks of the system are summarized in the Table 4.2 to 4.3. The first column of the first peak represents the percentage improvement in the performance using Feedforward controller compared to the original aircraft. And it is calculated by

$$Improvement using FF = \frac{peak of the original aircraft - peak using FF}{peak of the original aircraft} * 100 \tag{4.4}$$

Performance improvement using the SISO controller is presented in the 2nd column and it is calculated by

$$Improvement using SISO = \frac{peak using FF - peak using SISO}{peak using FF} * 100 \tag{4.5}$$

The negative values in the tables mean that there is a rise in the peak than expected. And the positive value tells the percentage improvement in the performance. From the tables it can be seen that using feedforward action at short gust lengths significantly increases the 2nd peak, but with the use of SISO controller with feedforward action improves the performance by reducing the 1st and 2nd peak.

From the Figure 4.10 to 4.19, it can be seen that at shorter gust lengths the feedforward controller is not very effective instead it excites the 2nd wing root significantly (cyan line) compared to the original aircraft (blue line). Along with the using the SISO controller the performance of the aircraft improves. At shorter gust lengths the SISO controllers are improving the feedforward controller's performance significantly (red line) in terms of reducing wing root moments M_x and M_y. At longer gust lengths the SISO controller is giving a better performance than the original aircraft. While using the SISO controller the basic flight parameter such as q, θ, α response were also recorded and it was found stabilizing for all gust and mass cases (please find Appendix A for k =1 case). One important observation from the plots and tables is that the performance of the controller improves from Mass cases 6-1. Which means that the controller performs better in the low mass cases compared to full aircraft, this a very practical controller because in real when the aircraft will cruise the mass of the aircraft will reduce due to fuel burn.

	K=1				K =2				K =3			
	1st Peak		2nd Peak		1st Peak		2nd Peak		1st Peak		2nd Peak	
Mass Case	FF (%)	SISO (%)	FF (%)	SISO (%)	FF (%)	SISO (%)	FF (%)	SISO (%)	FF (%)	SISO (%)	FF (%)	SISO (%)
1	32.49	2.82	-434.51	21.54	25.40	16.82	-268.15	24.90	25.63	15.29	-178.64	31.13
2	43.91	6.42	-700.65	21.06	29.73	27.15	-397.74	27.90	31.68	14.43	-240.02	34.45
3	2.22	27.90	-678.94	17.14	20.81	10.23	-418.63	23.01	17.84	10.28	-254.08	28.32
4	18.56	-0.15	-779.63	13.79	6.46	32.98	-428.14	18.71	27.29	15.20	-262.97	23.65
5	-1.49	0.45	-680.15	12.86	6.22	10.89	-411.20	18.39	19.32	13.11	-228.26	23.36
6	2.64	2.93	-669.94	14.79	12.88	17.88	-375.07	20.50	21.70	10.49	-222.89	25.72

	K=4				K =5				K =6			
	1st Peak		2nd Peak		1st Peak		2nd Peak		1st Peak		2nd Peak	
Mass Case	FF (%)	SISO (%)	FF (%)	SISO (%)	FF (%)	SISO (%)	FF (%)	SISO (%)	FF (%)	SISO (%)	FF (%)	SISO (%)
1	26.10	22.86	-120.12	34.58	27.55	23.61	-87.39	49.82	28.97	30.25	-63.79	59.96
2	33.42	27.88	-146.97	39.79	36.99	24.33	-95.27	47.38	37.53	31.10	-58.83	55.29
3	22.65	25.57	-154.54	37.18	28.33	25.59	-99.58	43.80	32.71	29.16	-60.75	51.17
4	34.56	27.29	-154.87	29.78	42.53	36.44	-94.74	36.31	50.82	44.01	-51.84	155.56
5	27.21	21.02	-131.44	30.07	35.65	30.71	-76.40	36.92	44.17	37.22	-36.57	46.15
6	27.66	17.63	-122.55	32.09	34.83	184.85	-66.02	155.54	42.43	22.88	-25.18	50.68

	K=7				K =8				K =9			
	1st Peak		2nd Peak		1st Peak		2nd Peak		1st Peak		2nd Peak	
Mass Case	FF (%)	SISO (%)	FF (%)	SISO (%)	FF (%)	SISO (%)	FF (%)	SISO (%)	FF (%)	SISO (%)	FF (%)	SISO (%)
1	32.26	34.23	-43.24	67.45	37.14	35.24	-5.76	68.46	37.14	35.17	-5.76	68.35
2	42.62	34.53	-28.63	62.31	52.28	34.55	23.91	56.37	52.26	40.28	23.91	57.05
3	39.70	32.36	-28.43	59.65	52.99	32.68	31.09	60.06	52.99	41.31	31.09	61.79
4	58.68	52.57	-16.25	55.90	70.82	50.71	47.68	51.68	70.82	52.13	47.68	51.25
5	52.46	158.03	-3.67	55.66	64.48	92.93	54.83	71.53	64.48	31.73	54.83	78.73
6	49.31	22.09	8.61	69.25	57.05	20.23	68.50	33.28	57.05	21.13	68.50	30.49

Mass Case			1	2	3	4	5	6
K = 10	1st Peak	FF (%)	39.86	56.83	61.96	63.32	57.58	46.24
		SISO (%)	31.09	28.45	20.30	-8.59	-3.26	6.58
	2nd Peak	FF (%)	25.14	57.12	78.70	70.71	81.34	82.91
		SISO(%)	36.03	2.32	-70.30	-1.06	7.51	134.08

TABLE 4.2: Comparison of Peak Reduction in Wing Root Moment,M_x,between Original Aircraft, Feedforward Action and Feedforward Action with SISO Controllers.

	K=1				K =2				K =3			
	1st Peak		2nd Peak		1st Peak		2nd Peak		1st Peak		2nd Peak	
Mass Case	FF (%)	SISO (%)	FF (%)	SISO (%)	FF (%)	SISO (%)	FF (%)	SISO (%)	FF (%)	SISO (%)	FF (%)	SISO (%)
1	13.69	15.87	-393.75	336.02	15.18	30.58	-223.19	24.37	18.08	27.41	-153.37	28.80
2	0.09	31.30	-644.70	22.19	19.13	36.59	-373.68	28.65	25.57	26.79	-238.35	33.95
3	0.00	29.67	17.10	18.11	2.07	28.03	-587.31	43.72	11.81	22.94	464.24	29.53
4	0.00	0.00	-764.34	15.31	-1.32	9.61	-415.59	21.67	14.40	21.22	-176.90	26.75
5	0.00	0.00	-704.76	15.30	2.84	12.63	-378.85	19.88	8.79	17.98	-177.39	25.07
6	0.00	0.00	-787.75	14.06	13.30	15.28	-397.06	20.37	13.22	6.84	-242.87	23.50

	K=4				K =5				K =6			
	1st Peak		2nd Peak		1st Peak		2nd Peak		1st Peak		2nd Peak	
Mass Case	FF (%)	SISO (%)	FF (%)	SISO (%)	FF (%)	SISO (%)	FF (%)	SISO (%)	FF (%)	SISO (%)	FF (%)	SISO (%)
1	22.19	39.80	-100.89	32.94	28.09	0.00	-72.52	0.00	28.45	46.98	-52.32	60.36
2	31.15	43.19	-35.41	39.29	37.41	46.19	-95.13	47.76	44.36	46.34	-57.45	56.56
3	20.55	36.55	-161.62	37.65	28.99	41.60	-104.24	44.23	38.98	35.75	-63.17	51.92
4	26.31	36.08	-153.61	33.74	36.96	44.09	-93.76	40.68	48.99	52.83	-50.67	48.78
5	22.39	35.09	-132.24	32.28	34.17	43.66	-76.76	39.08	47.24	50.02	-36.74	47.67
6	27.72	34.52	-134.62	29.59	40.13	46.15	-73.24	35.93	53.29	47.91	-29.28	44.78

	K=7				K =8				K =9			
	1st Peak		2nd Peak		1st Peak		2nd Peak		1st Peak		2nd Peak	
Mass Case	FF (%)	SISO (%)	FF (%)	SISO (%)	FF (%)	SISO (%)	FF (%)	SISO (%)	FF (%)	SISO (%)	FF (%)	SISO (%)
1	35.03	48.71	-34.40	71.70	43.06	47.24	1.34	63.19	43.06	48.10	1.34	59.10
2	47.33	50.27	-25.55	65.23	59.25	50.20	30.12	47.06	59.23	55.36	30.12	44.58
3	41.81	46.50	-28.53	60.86	60.22	46.96	33.59	59.69	60.22	59.72	33.59	54.64
4	56.99	62.62	-14.79	59.76	71.82	51.11	47.48	53.43	71.82	51.95	47.48	48.05
5	57.20	45.05	-3.55	59.41	70.61	29.05	52.48	63.61	70.61	29.64	52.48	57.31
6	64.93	36.55	6.29	59.12	70.89	30.45	62.01	29.21	70.89	31.06	62.01	7.14

Mass Case			1	2	3	4	5	6
K = 10	1st Peak	FF (%)	46.55	61.31	68.47	65.02	61.70	50.74
		SISO (%)	29.16	11.01	-7.24	-18.48	-13.84	1.09
	2nd Peak	FF (%)	31.09	60.16	75.63	67.78	69.73	54.51
		SISO (%)	20.46	-21.74	-65.87	13.44	-13.87	40.49

TABLE 4.3: Comparison of Peak Reduction in Wing Root Moment,M_y,between Original Aircraft, Feedforward Action and Feedforward Action with SISO Controllers.

4.3 LQR Controller Design

The final aircraft with the stabilizing TUV feedback controller had 121 states with 10 inputs and 9 outputs. After the classical approach advance Linear Quadratic Controller (LQR) was designed to reduce the wing bending. Flap 1 and Flap 2 was chosen as the stabilizing LQR control inputs and the outputs were tried to minimize. MATLAB was used to solve the Riccati equation. The linear-quadratic (LQ) state-feedback regulator was formed by output weighting, which minimized the quadratic cost function with output weighting defined by the equation

$$J(u) = \int_0^\infty (y^T \mathbf{Q} y + u^T \mathbf{R} u + 2y^T \mathbf{N} u) dt \tag{4.6}$$

the weighting matrices are defined by

$$\begin{bmatrix} \bar{Q} & \bar{N} \\ \bar{N}^T & \bar{R} \end{bmatrix} = \begin{bmatrix} C^T & 0 \\ D^T & I \end{bmatrix} \begin{bmatrix} Q & N \\ N^T & R \end{bmatrix} \begin{bmatrix} C & D \\ 0 & I \end{bmatrix} \tag{4.7}$$

In the first stage of the LQ controller design it was assumed that all the stated are measurable. Considering the above assumption, $\mathbf{Q}$ and $\mathbf{R}$ matrix were tuned to give the best performance. Figure 4.20 below shows the LQ control scheme. The best performance were found using the values

$$\mathbf{Q} = \begin{bmatrix} 1e-6 & 0 & 0 & 0 & 0 & 0 & 0 & 0 & 0 \\ 0 & 1e-4 & 0 & 0 & 0 & 0 & 0 & 0 & 0 \\ 0 & 0 & 1e-4 & 0 & 0 & 0 & 0 & 0 & 0 \\ 0 & 0 & 0 & 1e-4 & 0 & 0 & 0 & 0 & 0 \\ 0 & 0 & 0 & 0 & 1e-4 & 0 & 0 & 0 & 0 \\ 0 & 0 & 0 & 0 & 0 & 1e-8 & 0 & 0 & 0 \\ 0 & 0 & 0 & 0 & 0 & 0 & 1e-8 & 0 & 0 \\ 0 & 0 & 0 & 0 & 0 & 0 & 0 & 1e-6 & 0 \\ 0 & 0 & 0 & 0 & 0 & 0 & 0 & 0 & 1e-4 \end{bmatrix}$$

$$\mathbf{R} = \begin{bmatrix} 600000 & 0 \\ 0 & 1000000 \end{bmatrix}$$

Different mass cases (six mass cases) were varied along with the gust lengths (10 gust lengths). The rate limiters and the saturation point of the Flap 1 and 2 were also taken into account during the simulation. After the tuning of the Q and R as state-estimator was constructed to estimate the unmeasurable states. Among the total 121 states 104 states were measurable among the 121 measurable states it included the rigid body parameters such a q (pitch rate), θ (pitch angle), α angle of attack. The rest of the 17 flexible mode states were estimated using the Kalman filter and Kalman gain matrix L as defined in equation $2.14 - 2.19$ The Figure 4.21 shows the complete control scheme for the LQ controller with Kalman estimator.

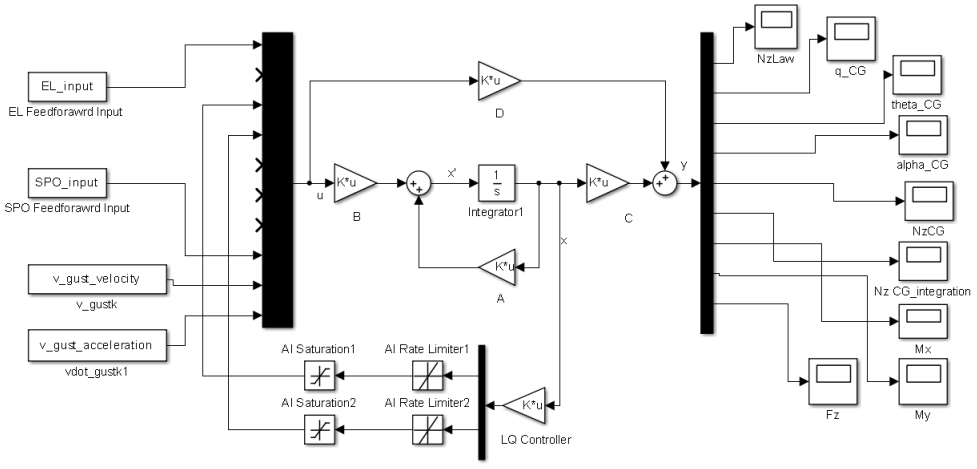

FIGURE 4.20: LQ Control Scheme.

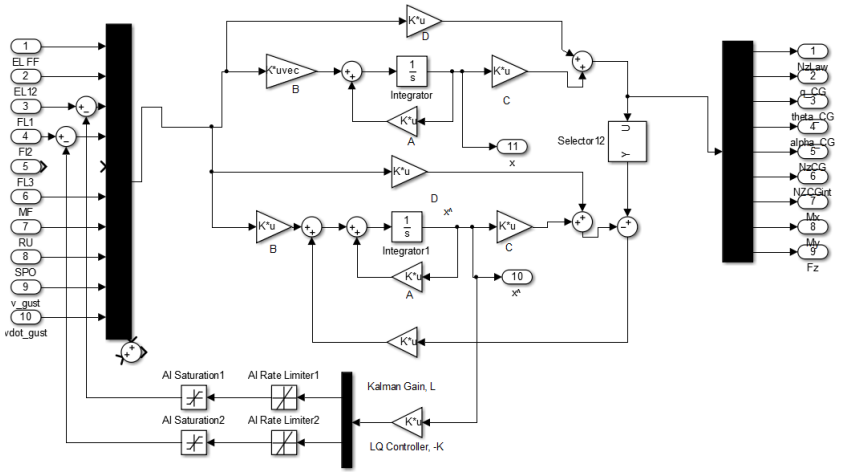

FIGURE 4.21: Complete LQ Control Scheme with Kalman Filter.

4.3.1 Performance Comparison Over Different Gust Lengths using LQ controller

Figure 4.22 to 4.31 shows the response of the wing root moments M_x and M_y for the gust cases k=1, 2, 5, 9, 10. All other gust cases had similar responses, please check appendix B. The cyan line corresponds to the original aircraft with TUV Feedback controller, blue line corresponds to aircraft with feedforward action and the red line corresponds to the aircraft with feedforward controller plus designed LQ controller to flap 1 and 2. Table 4.4 to 4.5 presents the summary of the peak improvements. The first column of the first peak represents the percentage improvement in the performance using feedforward controller compared to the original aircraft. And it is calculated by

$$ImprovementusingFF = \frac{peakoftheoriginalaircraft - peakusingFF}{peakoftheoriginalaircraft} * 100 \tag{4.8}$$

Performance improvement using the LQ controller is presented in the 2nd column and it is calculated by

$$ImprovementusingLQ = \frac{peakusingFF - peakusingLQ}{peakusingFF} * 100 \tag{4.9}$$

The negative values in the tables similarly as before mean that there is a rise in the peak. And the positive value tells the percentage improvement in the performance. If the Table 4.2, 4.3, 4.4 and 4.5 is compared it can be seen that SISO controller gives a better performance enhancement compared to LQ controller.

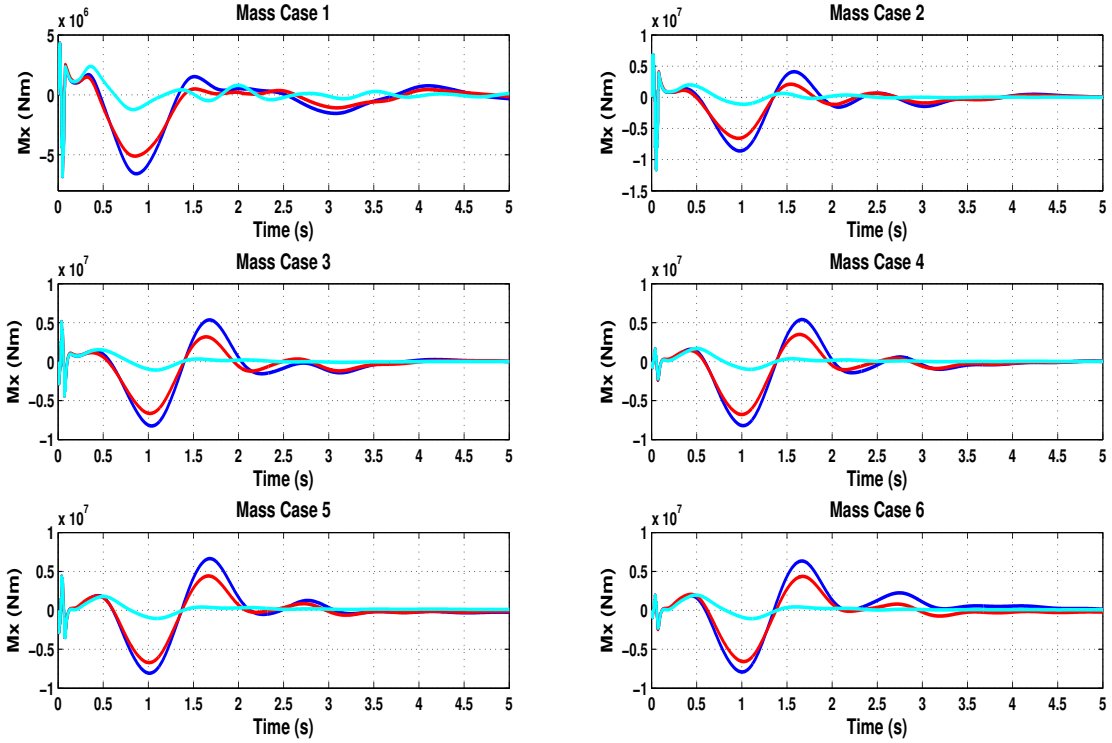

FIGURE 4.22: Wing Root Moment, M_x at gust length 9m (k=1) for different mass cases using LQ Controller.

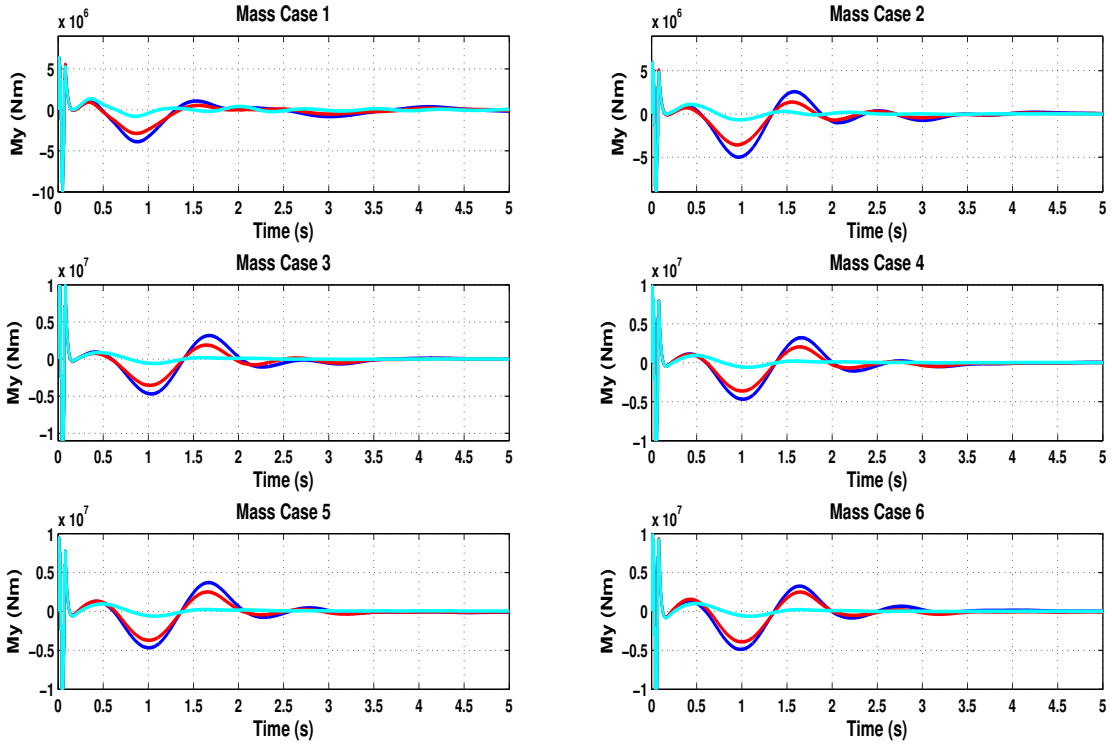

FIGURE 4.23: Wing Root Moment, M_y at gust length 9m (k=1) for different mass cases using LQ Controller.

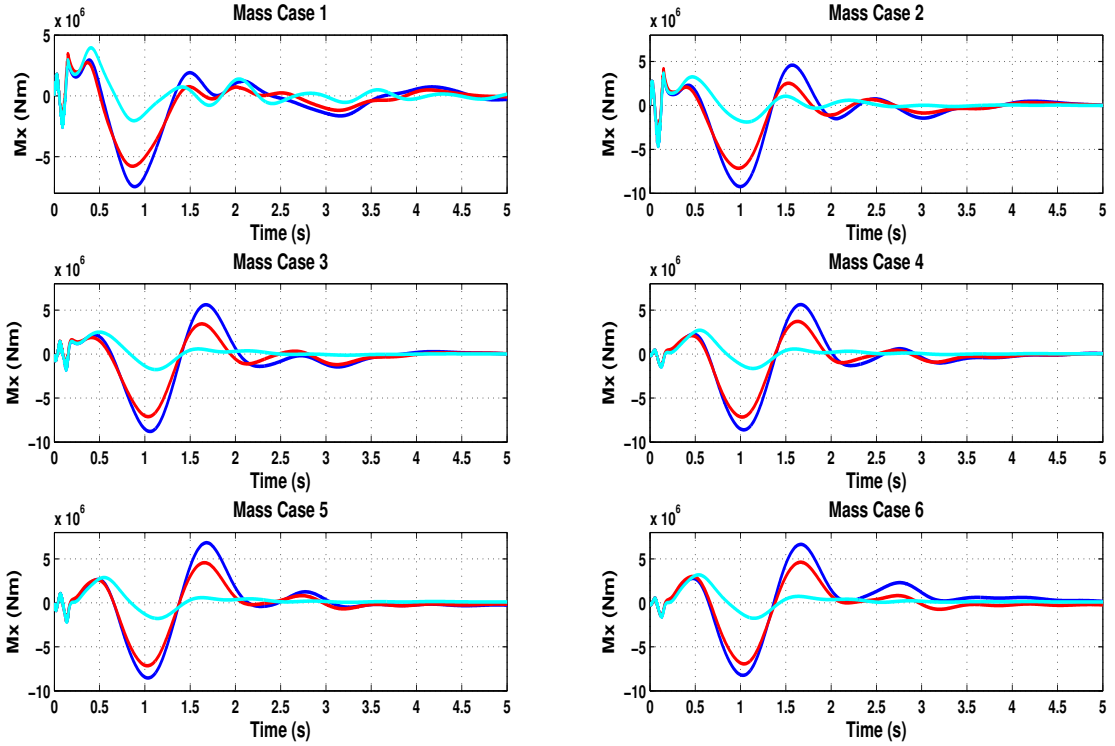

FIGURE 4.24: Wing Root Moment, M_x at gust length 18m (k=2) for different mass cases using LQ Controller.

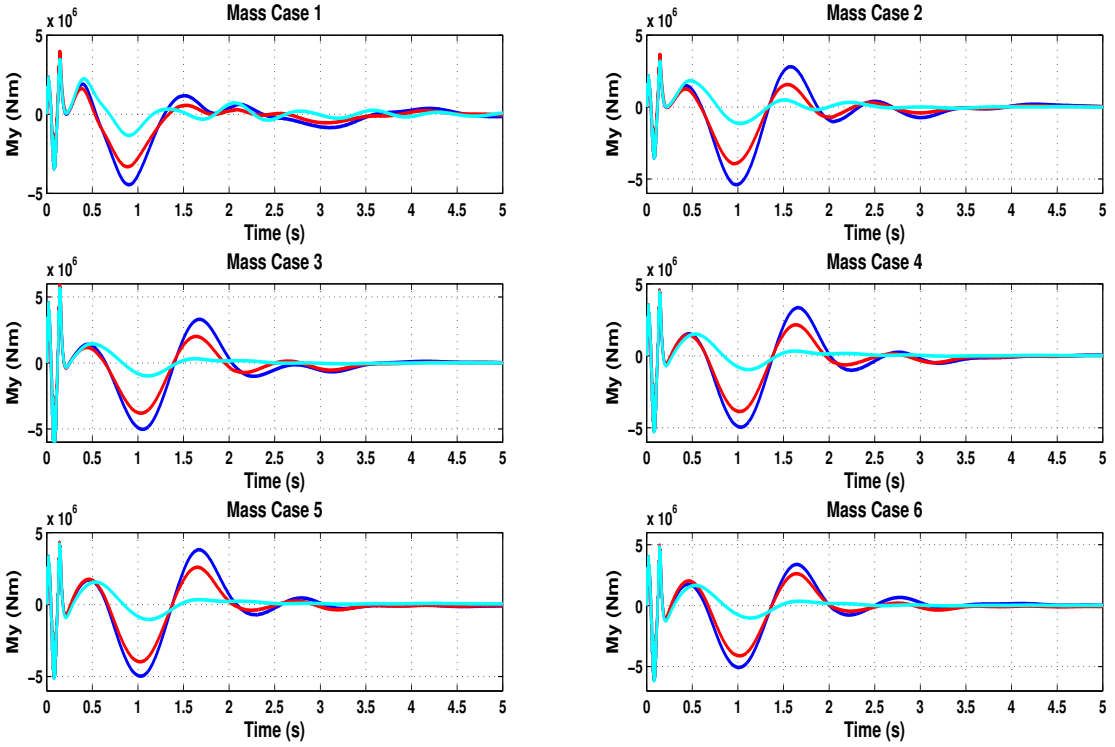

FIGURE 4.25: Wing Root Moment, M_y at gust length 18m (k=2) for different mass cases using LQ Controller.

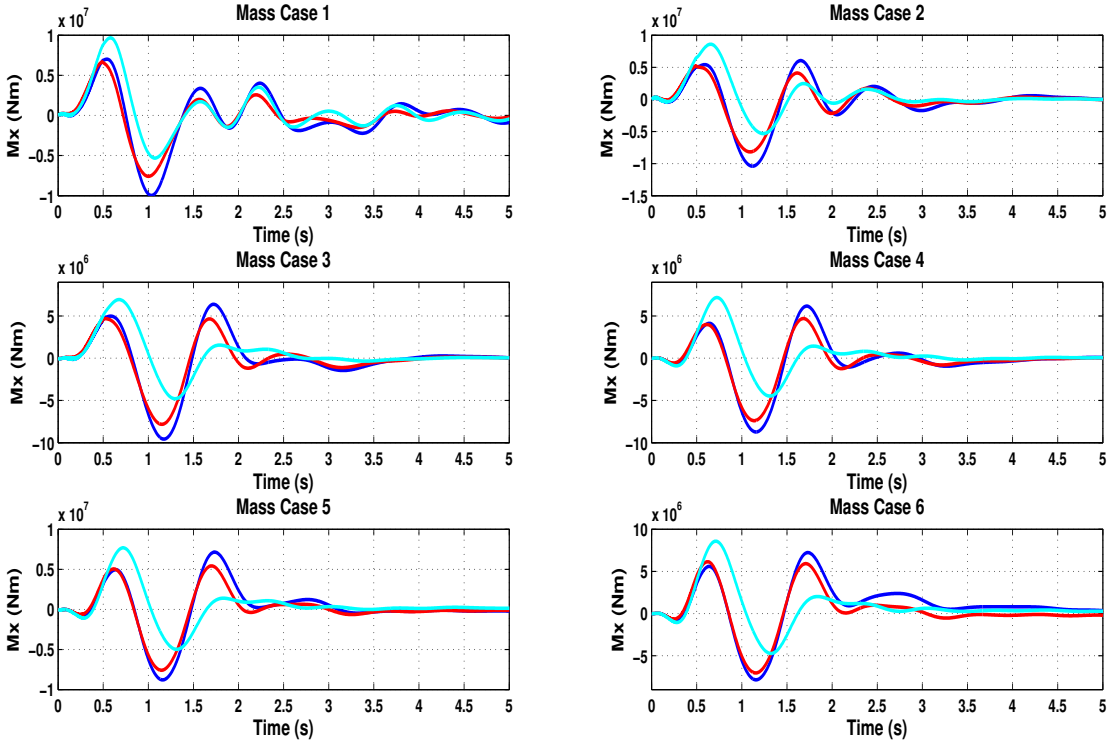

FIGURE 4.26: Wing Root Moment, M_x at gust length 60.96m (k=5) for different mass cases using LQ Controller.

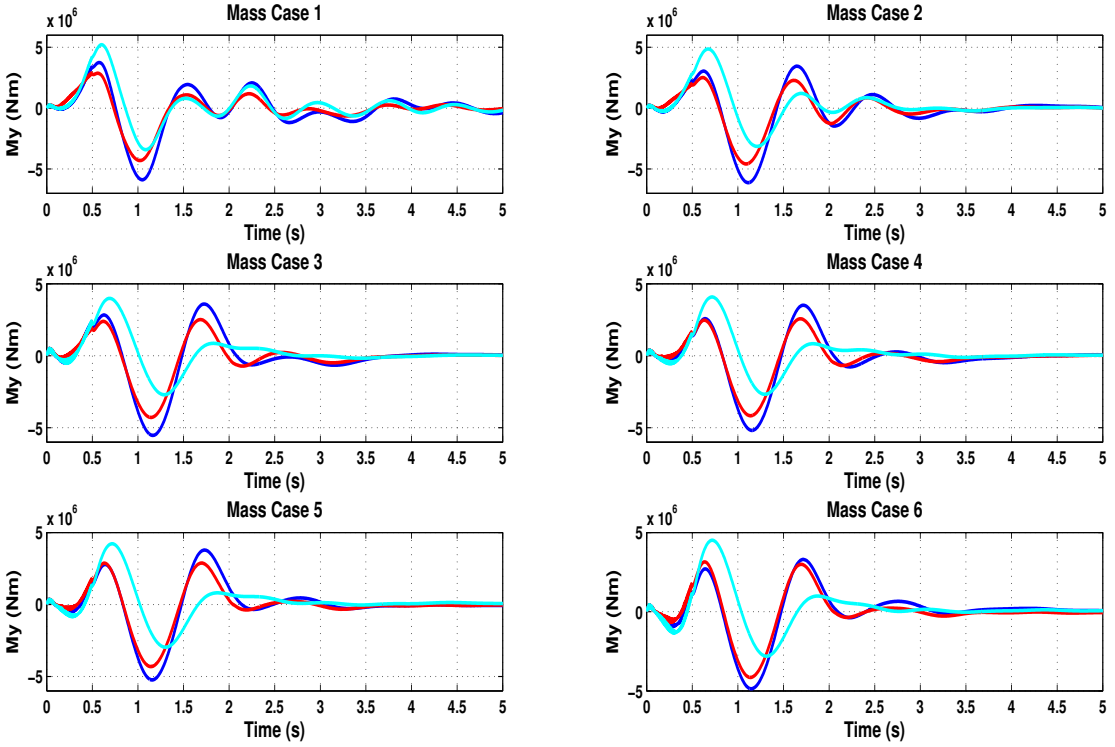

FIGURE 4.27: Wing Root Moment, M_y at gust length 60.96m (k=5) for different mass cases using LQ Controller.

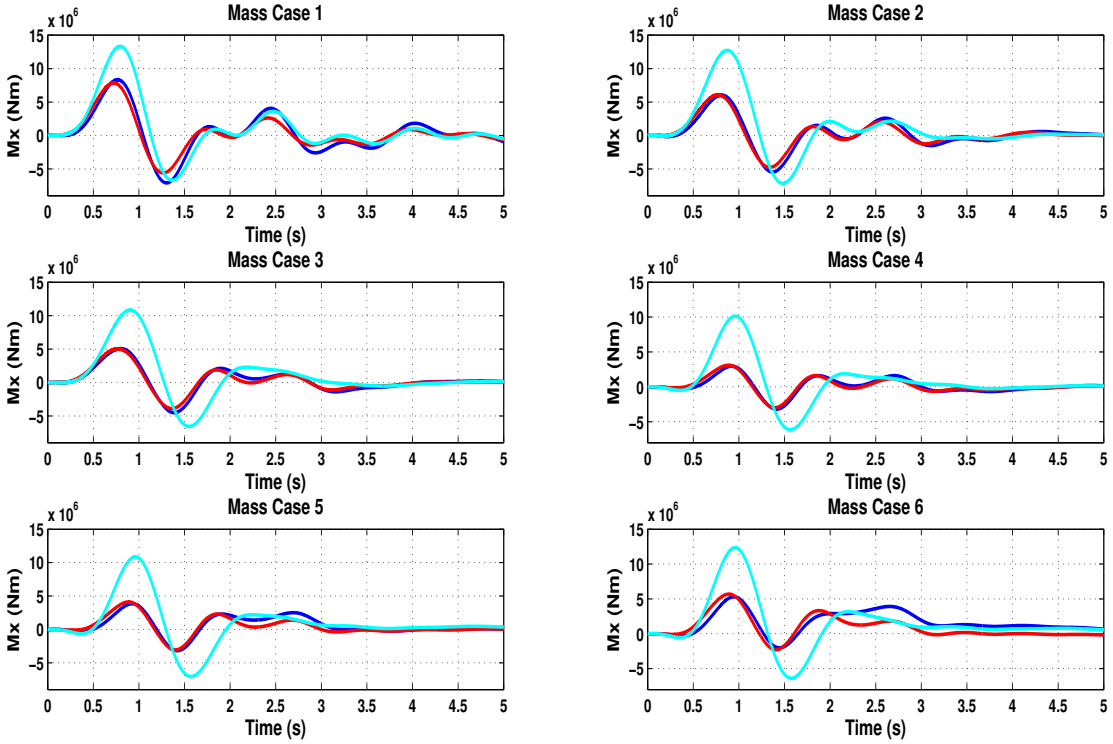

FIGURE 4.28: Wing Root Moment, M_x at gust length 121.92m (k=9) for different mass cases using LQ Controller.

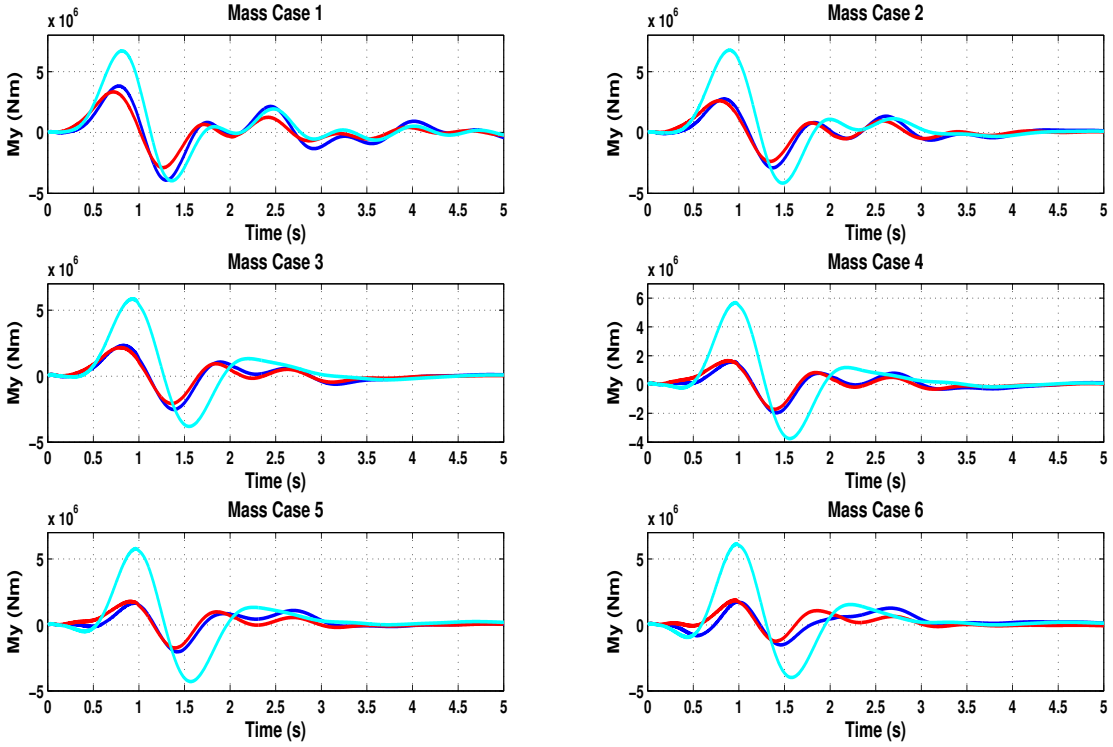

FIGURE 4.29: Wing Root Moment, M_y at gust length 121.92m (k=9) for different mass cases using LQ Controller.

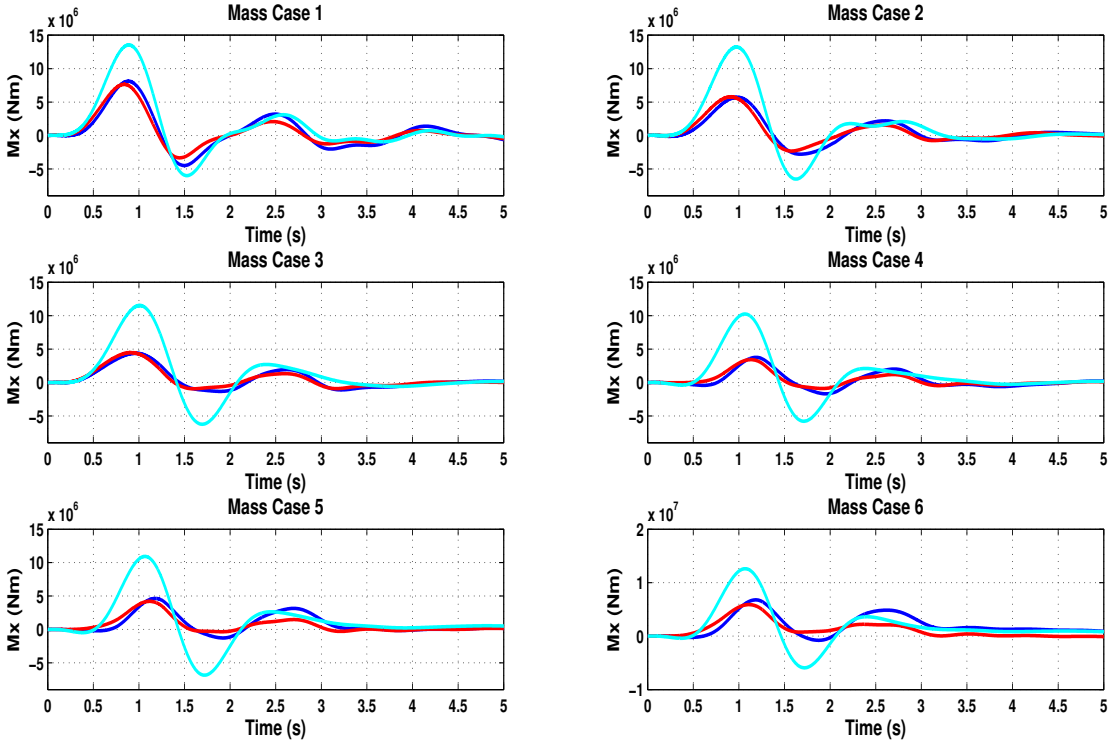

FIGURE 4.30: Wing Root Moment, M_x at gust length 152.4m (k=10) for different mass cases using LQ Controller.

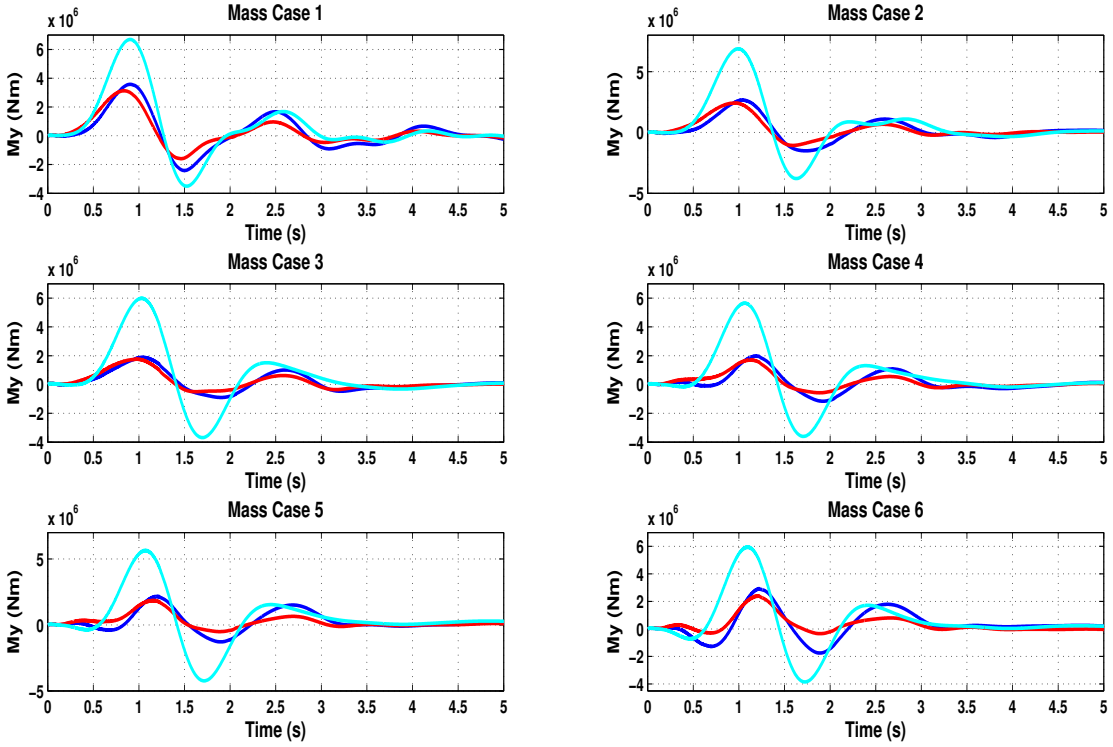

FIGURE 4.31: Wing Root Moment, M_y at gust length 152.4m (k=10) for different mass cases using LQ Controller.

	K=1				K =2				K =3			
	1st Peak		2nd Peak		1st Peak		2nd Peak		1st Peak		2nd Peak	
Mass Case	FF (%)	LQ (%)	FF (%)	LQ (%)	FF (%)	LQ (%)	FF (%)	LQ (%)	FF (%)	LQ (%)	FF (%)	LQ (%)
1	32.49	34.52	-434.51	21.91	25.40	8.73	-268.15	22.49	25.63	11.90	-178.64	23.76
2	43.91	41.02	-700.65	23.69	29.73	13.84	-397.74	22.57	31.68	12.30	-240.02	22.43
3	2.22	75.61	-678.94	20.34	20.81	13.47	-418.63	19.16	17.84	12.43	-254.08	18.85
4	18.56	15.74	-779.63	17.56	6.46	22.00	-428.14	16.94	27.29	6.54	-262.97	16.37
5	-1.49	0.00	-680.15	16.74	6.22	0.00	-411.20	16.27	19.32	0.74	-228.26	15.42
6	2.64	0.00	-669.94	16.96	12.88	0.00	-375.07	15.75	21.70	1.37	-222.89	14.17

	K=4				K =5				K =6			
	1st Peak		2nd Peak		1st Peak		2nd Peak		1st Peak		2nd Peak	
Mass Case	FF (%)	LQ (%)	FF (%)	LQ (%)	FF (%)	LQ (%)	FF (%)	LQ (%)	FF (%)	LQ (%)	FF (%)	LQ (%)
1	26.10	11.73	-120.12	24.33	27.55	4.75	-87.39	23.87	28.97	6.72	-63.79	23.06
2	33.42	11.80	-146.97	22.19	36.99	3.09	-95.27	21.35	37.53	4.63	-58.83	20.12
3	22.65	10.56	-154.54	18.68	28.33	6.69	-99.58	18.27	32.71	6.11	-60.75	17.80
4	34.56	4.87	-154.87	15.93	42.53	4.43	-94.74	15.27	50.82	0.17	-51.84	14.50
5	27.21	-0.41	-131.44	14.72	35.65	0.00	-76.40	13.70	44.17	-4.47	-36.57	12.54
6	27.66	-8.51	-122.55	12.59	34.83	0.00	-66.02	10.35	42.43	0.00	-25.18	7.47

	K=7				K =8				K =9			
	1st Peak		2nd Peak		1st Peak		2nd Peak		1st Peak		2nd Peak	
Mass Case	FF (%)	LQ (%)	FF (%)	LQ (%)	FF (%)	LQ (%)	FF (%)	LQ (%)	FF (%)	LQ (%)	FF (%)	LQ (%)
1	32.26	6.60	-43.24	21.99	37.14	5.75	-5.76	21.04	37.14	5.75	-5.76	21.04
2	42.62	3.84	-28.63	18.50	52.28	-0.79	23.91	12.66	52.26	-0.82	23.91	12.66
3	39.70	3.99	-28.43	17.19	52.99	1.04	31.09	13.42	52.99	1.04	31.09	13.42
4	58.68	-1.74	-16.25	13.54	70.82	201.01	47.68	196.91	70.82	-4.96	47.68	6.73
5	52.46	-5.76	-3.67	11.14	64.48	-6.71	54.83	3.30	64.48	-6.71	54.83	3.30
6	49.31	-13.02	8.61	3.72	57.05	-7.40	68.50	-14.30	57.05	-7.40	68.50	-14.30

Mass Case			1	2	3	4	5	6
K = 10	1st Peak	FF (%)	39.86	56.83	61.96	63.32	57.58	46.24
		LQ (%)	5.84	0.00	-2.85	8.96	9.10	13.01
	2nd Peak	FF (%)	25.14	57.12	78.70	70.71	81.34	82.91
		LQ (%)	25.66	18.10	30.27	49.26	75.57	1.38

TABLE 4.4: Comparison of Peak Reduction in Wing Root Moment,M_x,between Original Aircraft, Feedforward Action and Feedforward Action with LQ Controller.

	K=1				K =2				K =3			
	1st Peak		2nd Peak		1st Peak		2nd Peak		1st Peak		2nd Peak	
Mass Case	FF (%)	LQ (%)	FF (%)	LQ (%)	FF (%)	LQ (%)	FF (%)	LQ (%)	FF (%)	LQ (%)	FF (%)	LQ (%)
1	13.69	18.22	-393.75	26.05	15.18	15.26	-223.19	11.88	18.08	19.32	-153.37	26.35
2	0.09	42.76	-644.70	27.99	19.13	16.22	-373.68	27.22	25.57	6.92	-238.35	26.75
3	0.00	0.00	17.10	24.49	2.07	16.90	-587.31	3.25	11.81	16.09	464.24	23.76
4	0.00	0.00	-764.34	22.32	-1.32	5.88	-415.59	21.98	14.40	4.66	-176.90	21.22
5	0.00	0.00	-704.76	20.75	2.84	-2.92	-378.85	20.28	8.79	-3.50	-177.39	19.27
6	0.00	0.00	-787.75	19.82	13.30	0.00	-397.06	18.74	13.22	0.00	-242.87	17.44

	K=4				K =5				K =6			
	1st Peak		2nd Peak		1st Peak		2nd Peak		1st Peak		2nd Peak	
Mass Case	FF (%)	LQ (%)	FF (%)	LQ (%)	FF (%)	LQ (%)	FF (%)	LQ (%)	FF (%)	LQ (%)	FF (%)	LQ (%)
1	22.19	21.81	-100.89	26.83	28.09	22.77	-72.52	26.81	28.45	21.08	-52.32	26.30
2	31.15	17.31	-35.41	26.15	37.41	17.39	-95.13	25.13	44.36	17.17	-57.45	23.89
3	20.55	15.69	-161.62	23.77	28.99	15.59	-104.24	22.53	38.98	15.62	-63.17	21.79
4	26.31	4.71	-153.61	20.48	36.96	3.97	-93.76	19.57	48.99	3.27	-50.67	18.65
5	22.39	-2.82	-132.24	18.51	34.17	-3.53	-76.76	17.61	47.24	-4.61	-36.74	16.86
6	27.72	0.00	-134.62	16.14	40.13	0.00	-73.24	14.69	53.29	0.00	-29.28	13.37

	K=7				K =8				K =9			
	1st Peak		2nd Peak		1st Peak		2nd Peak		1st Peak		2nd Peak	
Mass Case	FF (%)	LQ (%)	FF (%)	LQ (%)	FF (%)	LQ (%)	FF (%)	LQ (%)	FF (%)	LQ (%)	FF (%)	LQ (%)
1	35.03	17.53	-34.40	25.58	43.06	12.77	1.34	26.12	43.06	12.77	1.34	26.12
2	47.33	14.77	-25.55	22.37	59.25	5.43	30.12	18.03	59.23	5.47	30.12	18.03
3	41.81	13.37	-28.53	20.89	60.22	6.94	33.59	17.96	60.22	6.94	33.59	17.96
4	56.99	-1.16	-14.79	17.53	71.82	0.00	47.48	12.38	71.82	-3.67	47.48	12.38
5	57.20	-9.59	-3.55	16.07	70.61	0.00	52.48	14.12	70.61	-5.28	52.48	14.12
6	64.93	-27.75	6.29	12.50	70.89	-6.98	62.01	18.31	70.89	-6.98	62.01	18.31

Mass Case			1	2	3	4	5	6
K = 10	1st Peak	FF (%)	46.55	61.31	68.47	65.02	61.70	50.74
		LQ (%)	12.54	9.05	6.81	13.83	14.21	18.17
	2nd Peak	FF (%)	31.09	60.16	75.63	67.78	69.73	54.51
		LQ (%)	34.05	29.49	44.81	50.37	60.16	80.34

TABLE 4.5: Comparison of Peak Reduction in Wing Root Moment,M_y,between Original Aircraft, Feedforward Action and Feedforward Action with LQ Controller.

4.4 $\mathcal{H}_\infty$ Controller Design

The aircraft dynamics was re-written in the general standard form as shown in Figure 2.2 and Equation 2.20. It was assumed that the only Flap 1 and 2 can be used to control the system and the outputs $\eta_z Law$, θ_{CG}, α_{CG}, η_{CG}, and q_{CG} are measurable. Figure 4.32 shows the control block diagram.

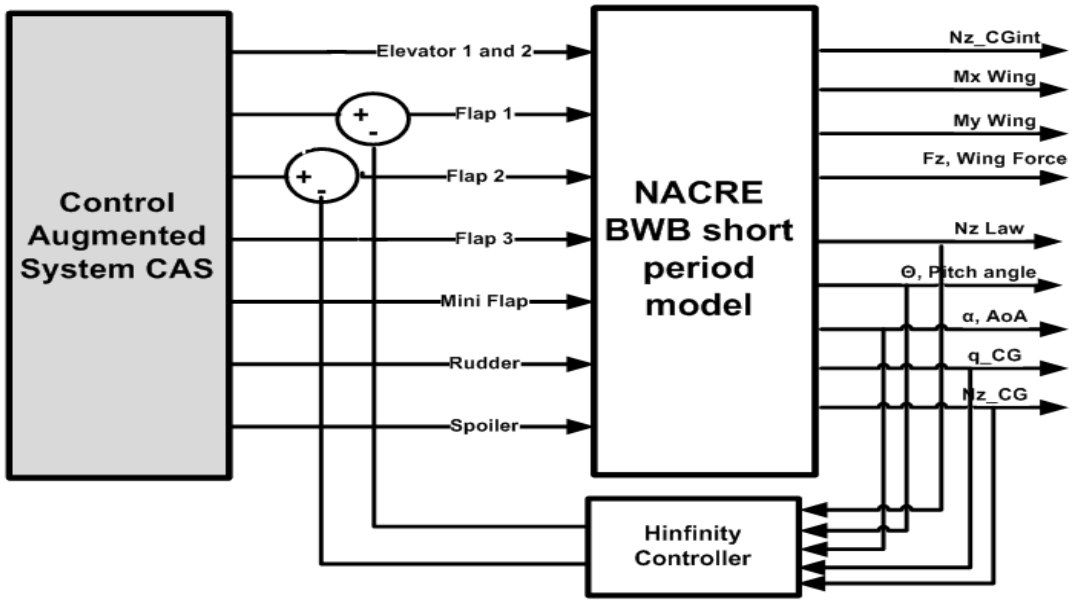

FIGURE 4.32: $\mathcal{H}_\infty$ Control Scheme.

The designed controller was stable and had 121 sates with 5 inputs as mentioned above. It had 2 outputs to Flap 1 and Flap 2. The performance of the controller was well without respecting the rate limits and saturation points. But when the actuator rate limiter and saturation points were set, the performance of the controller deteriorated. The performance of the controller is shown for gust cases 9m (k=1) and 152.4 m (k=10) in Figure 4.33 to 4.36.

From the plots, it can be seen that the $\mathcal{H}_\infty$ controller did not improve the performance of the gust load alleviation system significantly compared to the LQ controller and SISO controller. Therefore the designed $\mathcal{H}_\infty$ was ruled out from potential GLAS controller.

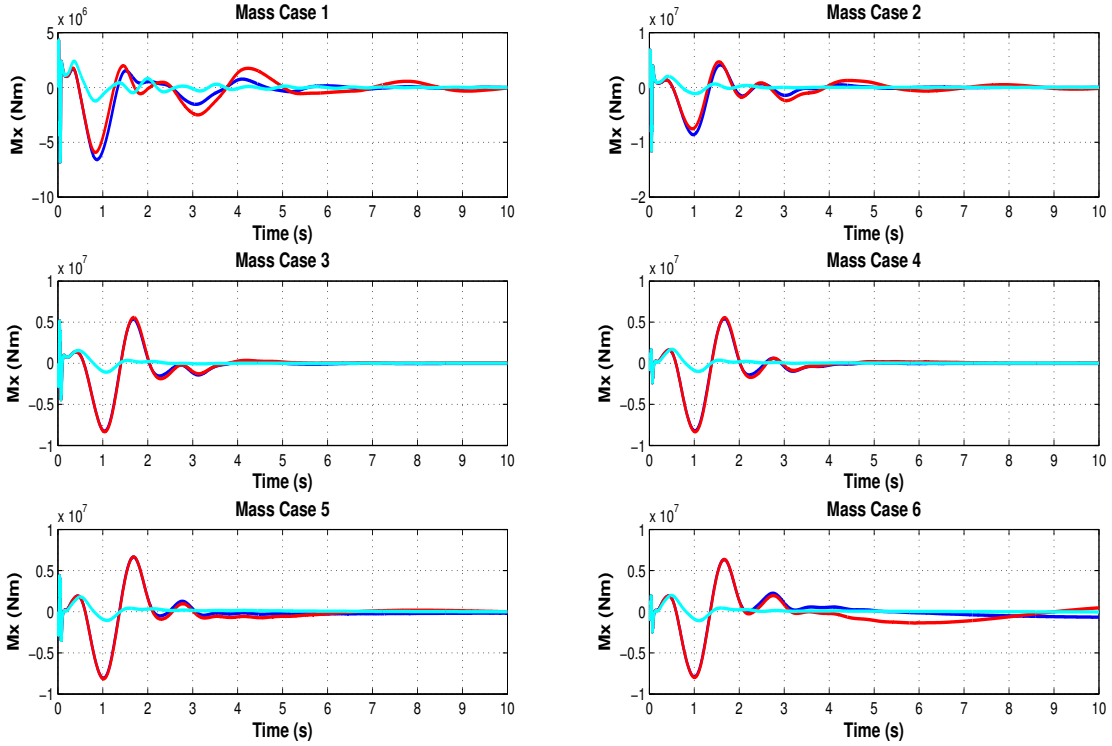

FIGURE 4.33: Wing Root Moment, M_x at gust length 9m (k=1) for different mass cases using $\mathcal{H}_\infty$ Controller.

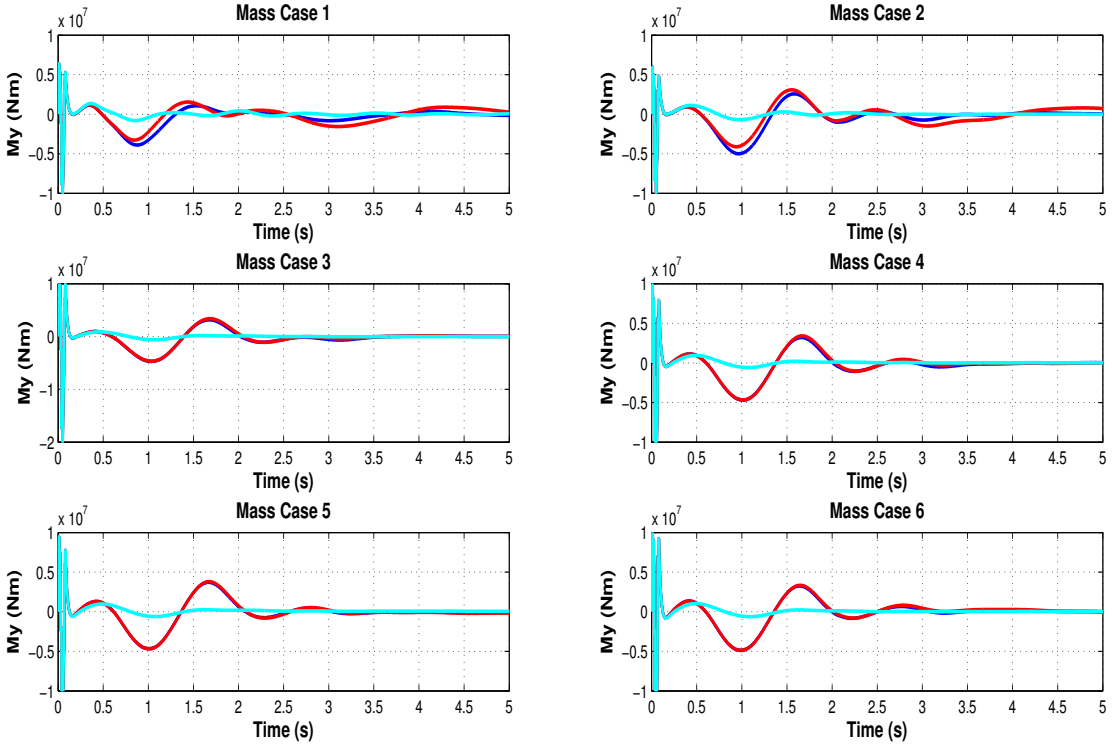

FIGURE 4.34: Wing Root Moment, M_y at gust length 9m (k=1) for different mass cases using $\mathcal{H}_\infty$ Controller.

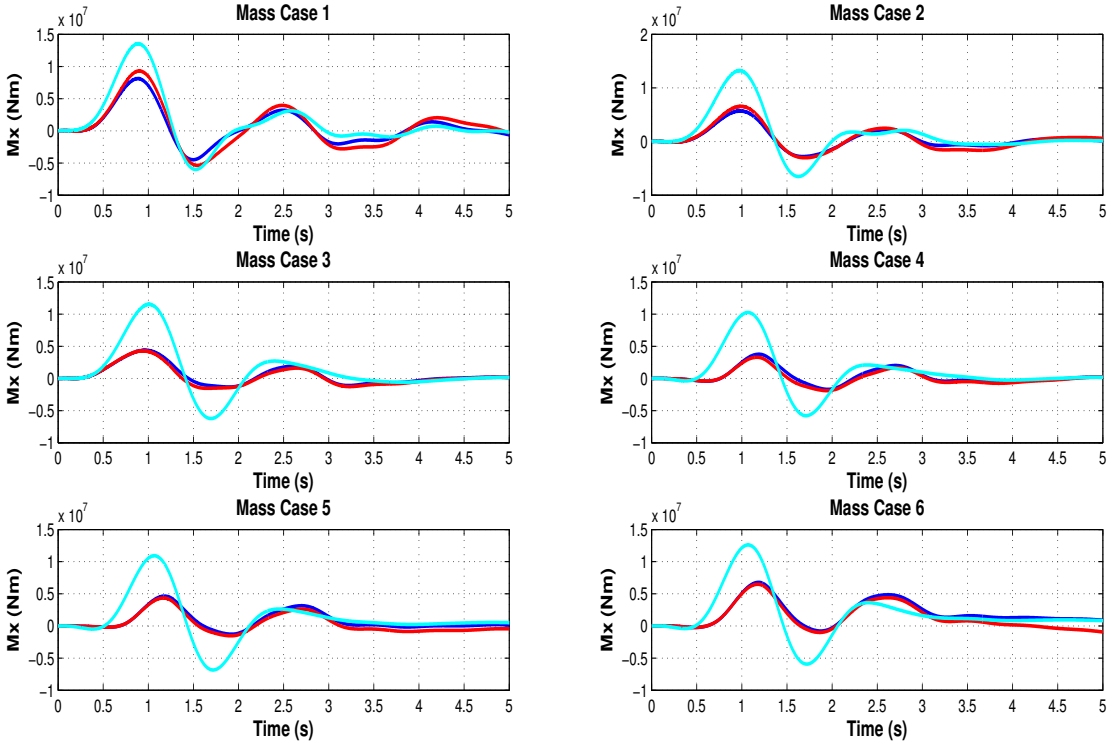

FIGURE 4.35: Wing Root Moment, M_x at gust length 152.4m (k=10) for different mass cases using $\mathcal{H}_\infty$ Controller.

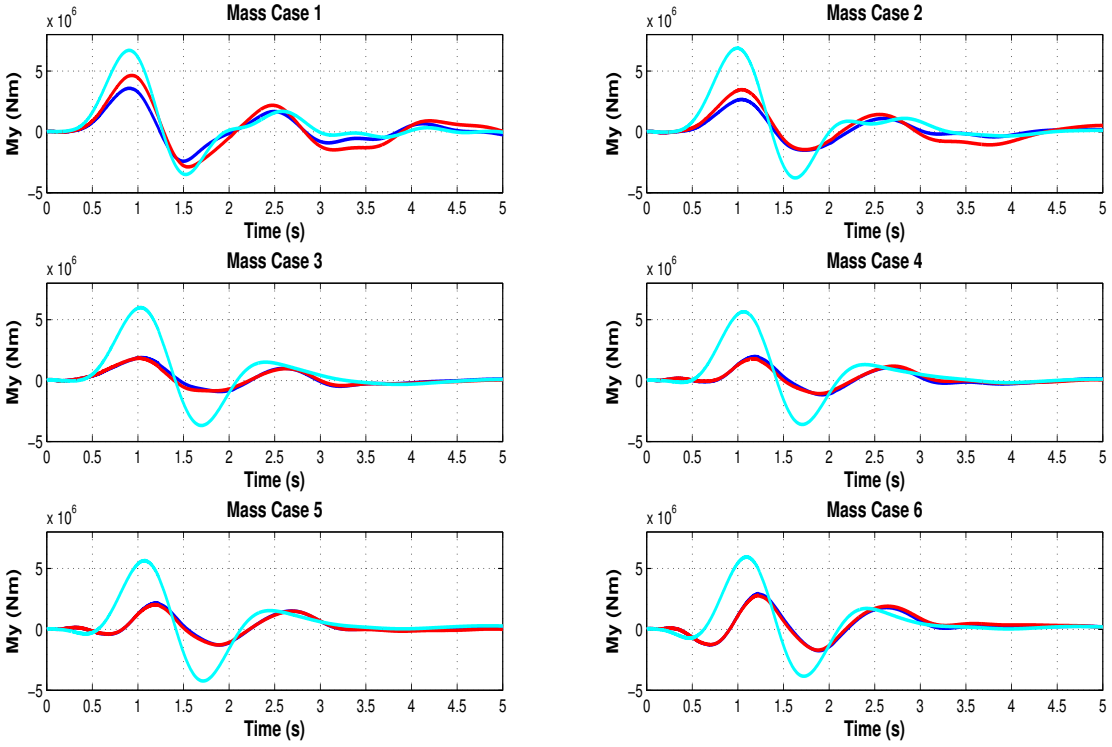

FIGURE 4.36: Wing Root Moment, M_y at gust length 152.4m (k=10) for different mass cases using $\mathcal{H}_\infty$ Controller.

Chapter 5

Discussion

5.1 Selection of Control Surfaces

If we look at the position of the actuators specifically Spoiler and Flaps, it can be seen that Flap 1 and Flap is right below Spoiler 1 and Spoiler 2. Now if we consider the feedforward control action by the spoiler in Figure 4.2 to alleviate the gust loading, it can be seen that the spoilers 1 and 2 deflects with a negative angle (which means the spoilers deflects upward) this produces a downward for force on the wing. This downward force on the wing gave rise to Wing root bending moment, M_x, and wing root torsional moment, M_y.

Therefore being Flap 1 and Flap 2 right below the spoilers; they would be the most efficient actuators to use. If the control actions in Figure 5.1 and 5.2 of the Flap 1 and Flap 2 is considered it can be seen that both the flaps deflects with a positive angle (which means the flaps deflects down), this produces a counter upward force on the wing which eventually reduces the Wing root bending moment M_x and wing root torsional moment, M_y. The figurs show the situation for the shortest gust load. The control action for other gust cases were the same.

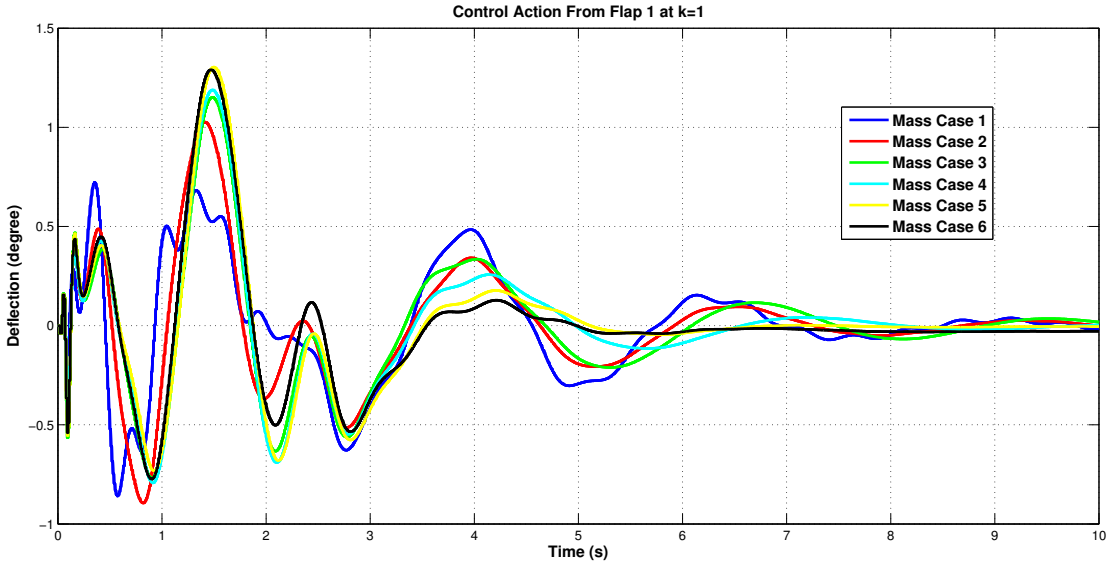

FIGURE 5.1: Flap 1 control action at gust length k=1.

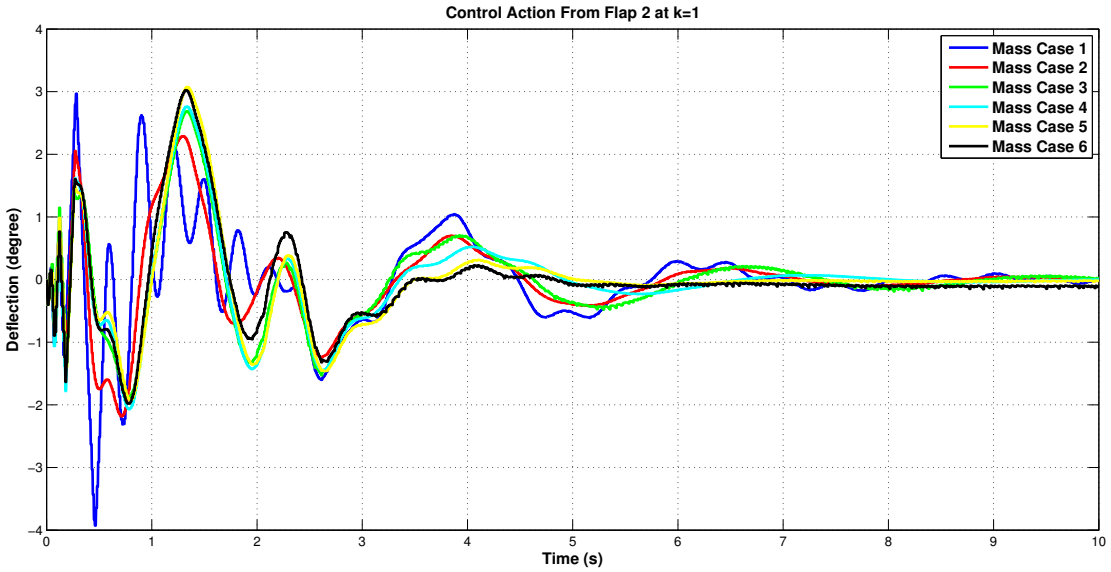

FIGURE 5.2: Flap 2 control action at gust length k=1.

5.2 Comparative Analysis between different Control Methods

In the Table 4.2- 4.5 it can be seen that the feedforward controller significantly excited the 2nd peak in both for both Mx and M_y. The feedforward controller gave a reasonable reduction in the $1st$ and 2nd peak for gust condition greater

than k =7. For shorter gust lengths than k=7 feedforward controller only did well to reduce the 1st peak. But while using the additional designed feedback controller with Flap 1 and Flap 2 it can be seen that for both the controller SISO and LQ the 1st and 2nd peak is reduced which indicates a performance improvement. While using the SISO controller the improvement is greater compared to LQ controller.

For the comparative analysis between the LQ and SISO controller the different mass cases were averaged for each gust lengths from Table 4.2 - 4.5. The obtained data is represented in Table 5.1 and 5.2.

Gust Cases	1st Peak		2nd Peak	
	LQ Controller (%)	SISO Controller (%)	LQ Controller (%)	SISO Controller (%)
K =1	27.82	6.73	19.53	16.86
K = 2	9.67	19.32	18.86	22.24
K = 3	7.55	13.13	18.50	27.77
K =4	5.01	23.71	18.07	33.91
K = 5	3.16	54.26	17.14	61.63
K = 6	2.19	32.44	15.91	69.80
K = 7	-1.01	55.63	14.35	61.70
K =8	32.15	44.39	38.84	56.90
K = 9	-2.19	36.96	7.14	57.94
K = 10	5.68	45.97	33.37	45.14

TABLE 5.1: Comparison of Average Peak Reduction in Wing Root Moment,M_x, for SISO controller and LQ controller.

Gust Cases	1st Peak		2nd Peak	
	LQ Controller (%)	SISO Controller (%)	LQ Controller (%)	SISO Controller (%)
K =1	10.16	12.81	23.57	70.17
K = 2	8.56	22.12	17.22	26.45
K = 3	7.25	20.53	22.47	27.93
K =4	9.45	37.54	21.98	34.25
K = 5	9.36	36.95	21.06	34.61
K = 6	8.75	46.64	20.14	51.68
K = 7	1.19	48.28	19.16	62.68
K =8	3.03	42.50	17.82	52.70
K = 9	1.54	45.97	17.82	45.14
K = 10	12.44	0.28	49.87	-4.51

TABLE 5.2: Comparison of Average Peak Reduction in Wing Root Moment,M_y, for SISO controller and LQ controller.

From the table it can be seen that SISO controller improves the feedforward performance significantly with respect to M_x and M_y compared to LQ controller. SISO controller exhibits superior reduction in the 1st peak and 2nd peak at shorter gust length.

The difficulty of using LQ controller remained with state estimation, the performance of the LQ controller degraded with Kalman state estimator. Perhaps better tuning of the LQ controller will give better results. The problem with optimal LQ controller tuning is that tuning these controller is not very intuitive. Its more like trial and error, which makes it difficult to use in Aerospace industry.

On the other hand SISO controller design is easy to implement and very intuitive in terms of designing. Therefore it makes it very safe to use in the Aerospace industry. In addition we do not need to estimate or measure all the states, this provides a greater economic advantage.

One another important consideration needs to be made, if the performance of the SISO controller is taken into account, it can be found that the performance improves from higher mass case to lower mass case. With respect to the reality, this controller is very practical because during cruise aircraft burns fuel and the mass reduces. As a result the performance of the SISO controller will get better along with the progress of the aircraft flight envelope.

Chapter 6

Conclusion

6.1 Summary of Thesis Achievements

ACARE vision 2020 was introduced to minimise the environmental effect of air traffic and to enable future aircraft industries growth. To meet the vision more aerodynamically efficient and light weight aircraft was required. As a result BWB flexible aircraft was developed. This light weight structures gave rise to significant flexibility issues. Therefore some sort of active structural damping was required when such NACRE BWB aircraft moves through gust/air turbulence.

The NACRE BWB aircraft model was provided by EADS Innovation Works. The non-linear model was linearised and was validated with linear model. The simulation showed very close match with the linearised approximations.

A feedforward control solution was patented to alleviate gust loading at EADS Innovations work, but the solution was not robust with respect to mass cases and gust length lower than 60.9 meter. The thesis work aimed toward developing a feedback controller which would increase the performance of the feedforward controller over shorter gust lengths upto 9 meter. Different feedback controller was investigated which included nominal SISO controller, linear quadratic controller and $\mathcal{H}_\infty$ controller. It was decided to use Flap 1 and Flap 2 as control surfaces for feedback controller.

SISO controller provided a superior performance at shorter gust lengths compared to LQ and $\mathcal{H}_\infty$ controller. For the SISO controller η_zLaw was feeded to Flap 1 and Flap 2. While designing the controller via root locus method frequency domain performance was taken into account so that the long period/Phugoid mode was not excited.

The performance of the LQ controller degraded with the addition of constraints such as rate limiter and saturation for Flap 1 and Flap 2. The difficulty with LQ controller also remained with state estimation. Comparatively SISO controller was easy to implement and respected the constraints imposed by the actuator. The control actions using the SISO controller were not very vigorous, so it provided a better simulation result in terms of reducing wing bending moment, M_x and torsional moment, M_y.

SISO controller was more efficient in lower mass cases than higher mass cases. The SISO controller had an improved performance over lower mass cases, which is practically very good because the aircraft cruises it burns fuel and the aircraft mass reduces.

6.2 Future Work

In future the thesis work can be carried forward by extending the optimal control strategy with Model Predictive Control (MPC) which will take the constrains such as rate limits and saturation points into account from the very beginning of the control algorithm.

Further better tuning of the LQ and $\mathcal{H}_\infty$ controller might also be useful in further simulation cases. Investigation on more flight regimes such as take-off, climb could be carried out. The low speed study of this type of aircraft is also essential to find its performance in the particular regime.

The thesis work can also be extended to other types of conceptual aircraft developed within the ACARE vision such as ACFA2020 BWB aircraft. Adaptive fault tolerant GLAS system can also be considered as a future work.

Appendix A

Response of the Basic Aircraft Parameter

The Figures below shows the aircraft's basic parameter's response to the controller. These parameter were also stabilized by the SISO and LQ controller. And the response looked similar. The plots shows the response for the SISO controller at shortest gust length. For all other gust lengths the plots were similar.

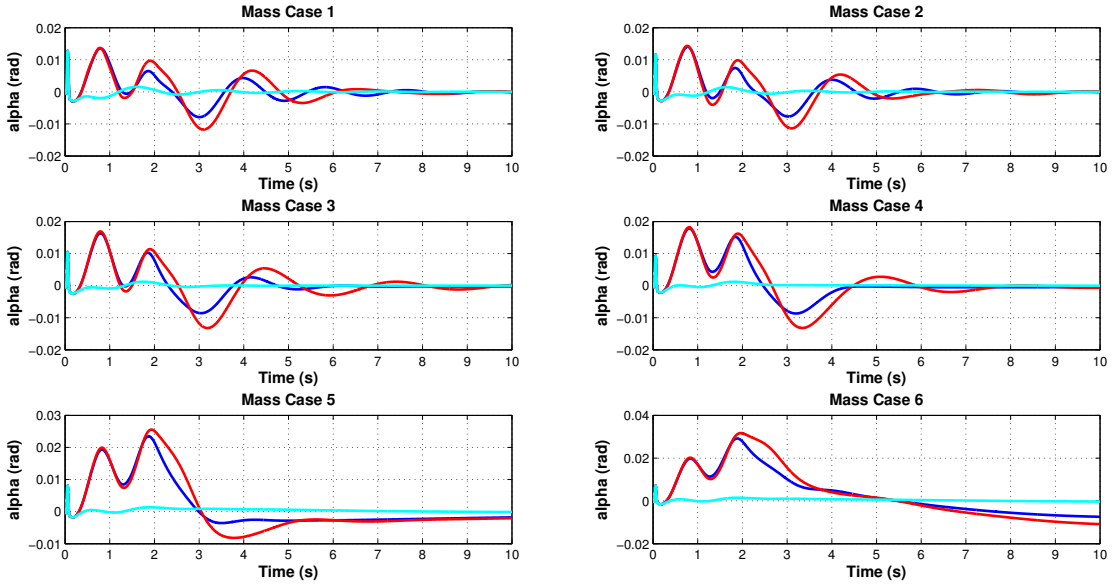

FIGURE A.1: α response at gust length k =1.

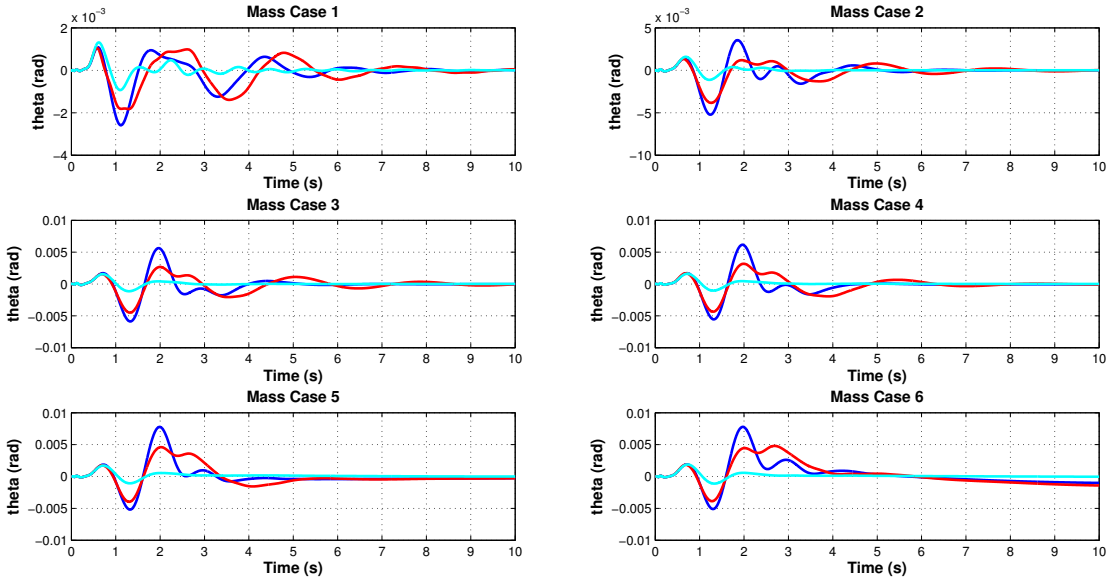

FIGURE A.2: θ response at gust length k =1.

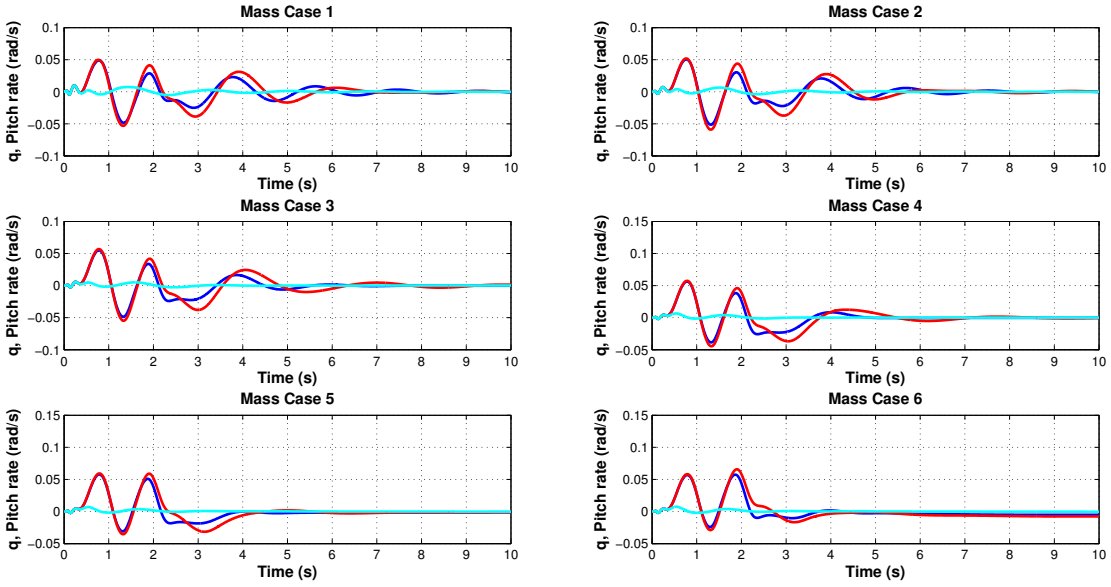

FIGURE A.3: q response at gust length k =1.

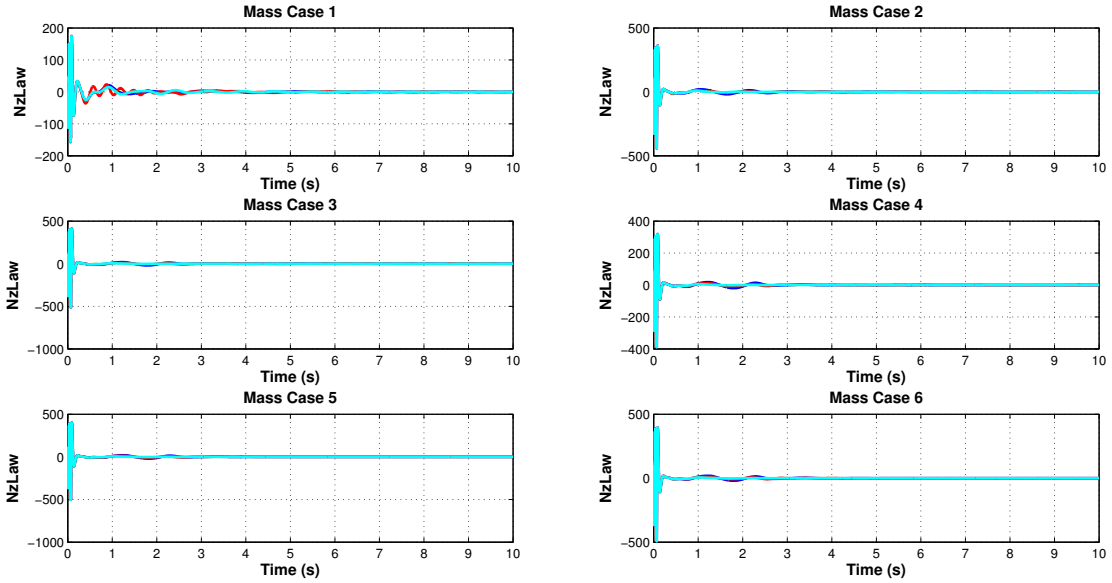

FIGURE A.4: η_zLaw response at gust length k =1.

Bibliography

[1] *ACFA 2020 an FP7 Project on Active Control of Flexible Fuel Efficient Aircraft Configurations*, 2011.

[2] R. H. Liebeck. Design of the blended wing body subsonic transport. *Journal of Aircraft*, 2003.

[3] Dale E. Seborg; Thomas F. Edgar; Duncan A. Mellichamp. *Process Dynamics and Control*. John Wiley and Sons, 2003.

[4] Felix; Klimmek Thomas; Sika Zbynek; Hanis Tomas; Valasek Michael; Gangsaas Dagfinn; Aversa Nicky; Berard Adrien Wildschek, Andreas; Stroscher. Gust load alleviation on a large blended wing body airliner. In *27th International Congress of The Aeronautical Sciences*, .

[5] Wildschek Tomas, Hanis; Andreas. *Methods and apparatus for minimizing dynamic structural loads of an aircraft*. EADS - IW European patent No 11175857-9-1239, Munich.

[6] J Frota. New aircraft concept research in nacre - a five-year synthesis (2005-2010). Technical report, Aerodays 2011, 2011.

[7] Felix; Hani Tom Wildschek, Andreas; Stroscher. Fuel management system for cruise performance optimisation on a large blended wing body airliner. *4TH European Conference for Aerospace Sciences (EUCASS)*, 2011.

[8] *Configuration selection for a 450 passenger ultra-efficient 2020 aircraft*, 2011.

[9] Anthony N. Antsaklis, Panos J.; Michel. *A Linear Systems Primer*. Birkhauser Boston, 2007.

[10] Cees Ikeda, Toshihiro; Bil. Aerodynamic performance of a blended wing body configuration aircraft. In International Congress Of The Aeronautical Sciences, editor, *25th International Congress of the Aeronautical Sciences*, 2006.

[11] A; Le Moigne A; Laban M; Hackett K; Weinerfelt P Qin, Q; Vavalle. Aerodynamic studies for blended wing body aircraft. In AIAA, editor, *9th AIAA/ISSMO Symposium on Multidisciplinary Analysis and Optimization*, 2002.

[12] A; Hemedi M; Kozek M Westermayer, C; Schirrer. An hinfinity full information approach for the feedforward controller design of a large bwb flexible aircraft. In *4th European Conference for Aerospace Sciences*.

[13] Arthur E. Bryson. *Control of Spacecraft and Aircraft*. Princeton University Press, 1994.

[14] Gianfranco; Dircken Frank Voskuijl, Mark; La Rocca. Controllability of blended wing body aircraft. In *26th International Congress of The Aeronautical Sciences*.

[15] Christoph Neubacher. Flight dynamic investigations of a blended wing body aircraft. Technical report, Hamburg University of Applied Sciences, 2008.

[16] Rudolf; Hromcik Martin; Hanis Tomas; Schirrer Alexander; Kozek Martin; Westermayer Christian; Hemedi Mark Wildschek, Andreas; Maier. Hybrid controller for gust load alleviation and ride comfort. In *3rd European Conference For Aerospace Sciences (EUCASS)*, .

[17] Martin Hanis, Tomas; Hromcik. Lateral control for flexible bwb high-capacity passenger aircraft. In *18th IFAC World Congress*, .

[18] V; Hromcik Martin Hanis, Tomas; Kucera. Low order hinfinity optimal control for acfa blended wing body aircraft. In *4th European Conference For Aerospace Sciences (EUCASS)*, .

[19] C; Hemedi M; Kozek M Schirrer, A; Westermayer. Lq-based design of the inner loop lateral control for a large flexible bwb-type aircraft. In *IEEE International Conference on Control Applications*.

[20] Marcel Sidi. *Spacecraft Dynamics and Control*. Cambridge University Press, 2000.

[21] Robert C. Nelson. *Flight Stability and Automatic Control*. McGrawHill, 1998.

[22] Brian L. Stevens; Frank L. Lewis. *Aircraft Control and Simulation*. Wiley-Interscience Publication, 1992.

[23] Jan Roskam. *Airplane Flight Dynamics and Automatic Flight Control*. DARcorp, 2001.

[24] Sigurd Skogestad; Ian Postlethwaite. *Multivariable Feedback Control: Design and Analysis*. John Wiley and Sons, 1996.

[25] Donald McLean. *Automatic Flight Control Systems*. Prentice Hall, 1990.

[26] Frank Lewis; Vassilis Syrmos. *Optimal Control*. John and Willey Sons, 1995.

[27] Tomas Hanis. *Active Control For High Capacity Flexible Aircraft*. PhD thesis, Czech Technical University, 2012.